

# Effective theory of the $\Delta(1232)$ in Compton scattering off the nucleon

Vladimir Pascalutsa\* and Daniel R. Phillips†

*Department of Physics and Astronomy,  
Ohio University, Athens, OH 45701*

(Dated: October 9, 2018)

## Abstract

We formulate a new power-counting scheme for a chiral effective field theory of nucleons, pions, and Deltas. This extends chiral perturbation theory into the Delta-resonance region. We calculate nucleon Compton scattering up to next-to-leading order in this theory. The resultant description of existing  $\gamma p$  cross section data is very good for photon energies up to about 300 MeV. We also find reasonable numbers for the spin-independent polarizabilities  $\alpha_p$  and  $\beta_p$ .

PACS numbers: 13.60.Fz - Elastic and Compton scattering. 14.20.Dh - Proton and neutrons. 25.20.Dc - Photon absorption and scattering

arXiv:nucl-th/0212024v4 15 Mar 2003

---

\*Electronic address: vlad@phy.ohiou.edu

†Electronic address: phillips@phy.ohiou.edu

## I. INTRODUCTION

Compton scattering on the proton ( $\gamma p$ ) and the deuteron ( $\gamma D$ ) provides a clean and unique probe of nucleon electromagnetic structure, revealing information different to that obtained in electron scattering. During the past decade a number of excellent experimental programs have been dedicated to these two processes (see Refs. [1–5] and [6–10], respectively). At low photon energies, these experiments probe the static properties of the nucleon, such as its electric charge, magnetic moment, and polarizabilities. Above the pion-production threshold, the process becomes dominated by the excitation of resonances, most prominently the  $\Delta(1232)$ -isobar. Many theoretical methods aim at understanding this process in both the low-energy and the resonance region. In particular, significant progress has been made recently using dispersion relations [11, 12] and effective Lagrangian models [13–15]. On the other hand, previous calculations using chiral perturbation theory ( $\chi$ PT) appear to work only at low photon energies—energies at or below the pion-production threshold [16, 17]. This present study attempts to extend these  $\chi$ PT calculations above the pion threshold and into the Delta-resonance region.

In the low-energy regime  $\chi$ PT seems to work extremely well. At next-to-leading order (NLO), i.e., third order in small momenta [=  $O(q^3)$ ], heavy-baryon (HB)  $\chi$ PT predicts, for the electric and magnetic polarizabilities [18, 19]:

$$\alpha_p = \alpha_n = \frac{5\pi\alpha}{6m_\pi} \left( \frac{g_A}{4\pi f_\pi} \right)^2 = 12.2 \times 10^{-4} \text{ fm}^3, \quad (1)$$

$$\beta_p = \beta_n = \frac{\pi\alpha}{12m_\pi} \left( \frac{g_A}{4\pi f_\pi} \right)^2 = 1.2 \times 10^{-4} \text{ fm}^3, \quad (2)$$

where  $\alpha = e^2/4\pi \simeq 1/137$ ,  $g_A \simeq 1.26$ ,  $f_\pi \simeq 93$  MeV,  $m_\pi \simeq 139$  MeV [47]. Since there are no Compton counter-terms present at  $O(q^3)$ , this is a genuine prediction of  $\chi$ PT. A prediction which—at least for the proton—is in remarkable agreement with recent extractions of these quantities from low-energy data, e.g. [20]:

$$\alpha_p = (12.1 \pm 1.1 \pm 0.5) \times 10^{-4} \text{ fm}^3, \quad (3)$$

$$\beta_p = (3.2 \pm 1.1 \pm 0.1) \times 10^{-4} \text{ fm}^3, \quad (4)$$

where the first error is statistical and the second represents the theory error of the fit to data.

However, the agreement of the NLO HB $\chi$ PT prediction with the experimental  $\gamma p$  cross-section data is good only up to photon energies  $\omega \simeq 100$  MeV [16]. The recent NNLO [ $O(q^4)$ ] calculation [17] agrees with experiment to slightly higher energies, but above  $\omega \simeq 120$  MeV significant discrepancies begin to appear, most notably at backward angles. This is perhaps not surprising, since the Delta-isobar excitation is not included explicitly in this chiral expansion. And, as we shall argue, the breakdown scale of  $\chi$ PT without an explicit Delta is set essentially by the Delta-nucleon mass difference:

$$\Delta \equiv M_\Delta - M_N \approx 293 \text{ MeV}. \quad (5)$$

Thus, to extend the region of  $\chi$ PT applicability to  $\omega \sim \Delta$ , the Delta must be included as an explicit degree of freedom.

The Delta contribution for the Compton amplitude had already been analyzed using chiral effective Lagrangians with explicit Deltas in Refs. [21–23]. These studies focused mainly on nucleon polarizabilities. The predictions made in Refs. [19, 21, 22] are obscured by off-shell ambiguities, in particular by the so-called “*off-shell parameters*” which control the infamous spin-1/2 sector of the spin-3/2 Delta field. In a “reasonable” range for these parameters the Delta contribution to  $\beta_p^{(\Delta)}$  varies between 0 and  $14 \times 10^{-4} \text{ fm}^3$  [22]. In contrast, Hemmert *et. al.* [23], to next-to-leading order in their *small scale expansion* (SSE) [24], find a result which is independent of the off-shell parameters, and thus is apparently a reliable prediction. But this prediction for the Delta-contribution to the magnetic polarizability is  $\beta_p^{(\Delta)} \approx 9 \times 10^{-4} \text{ fm}^3$ , in dramatic contradiction with experiment [25]. (For an attempt to remedy this using a “modified SSE” see Ref. [26].)

In this work we include the Delta in the chiral Lagrangian in a fashion somewhat different to this literature. First of all, the Lagrangian is written such that the unphysical spin-1/2 components of the Delta field decouple from observables [27, 28], hence no “off-shell parameters” appear. This feature of our Lagrangian, besides removing the redundant parameters, allows us to dress the Delta-pole contribution in a manifestly covariant way.

Furthermore, we set up our power-counting scheme so that it is both closely connected to the usual  $\chi$ PT without explicit Deltas in the low-energy region  $\omega \sim m_\pi$ , and extends to the Delta region  $\omega \sim \Delta$ . This is achieved by recognizing the hierarchy of scales:

$$m_\pi \ll \Delta \ll \Lambda \sim 1 \text{ GeV}, \quad (6)$$

where  $\Lambda$  stands for the “high-energy scale”, the breakdown scale of the theory. Therefore, our scheme is rather different from the SSE of Refs. [23, 24] (see also Ref. [29]), where the Delta-nucleon mass-difference is assumed to be of order  $m_\pi$  (i.e.,  $\Delta \sim m_\pi$ ). A more detailed comparison of our scheme and the SSE will be given below.

With the three-scale hierarchy (6) one in principle has two small expansion parameters:  $m_\pi/\Delta$  and  $\Delta/\Lambda$ . We regard both of them as roughly the same size and so introduce a single small parameter:

$$\delta = \frac{\Delta}{\Lambda} \sim \frac{m_\pi}{\Delta}. \quad (7)$$

Note that this implies that  $m_\pi$  scales as  $\delta^2$ .

The validity of the scale hierarchy (6) and the expansion in powers of  $\delta$  (which we shall refer to as the  $\delta$ -*expansion*) is to be judged by the success of the resultant effective-field-theory (EFT) description of processes involving the excitation of Delta. We regard the results we shall present here for  $\gamma p$  scattering as significant evidence in favor of this EFT expansion.

To obtain the NLO result for  $\gamma N$  scattering in our scheme for both the low-energy and the Delta regions, the Delta-pole contribution to this process must be dressed, and then added to the NLO HB $\chi$ PT result. This introduces two free parameters which characterize the strength of the  $\gamma N \rightarrow \Delta$  transition:  $g_M$  and  $g_E$ . Adjusting these parameters we find very good agreement with the experimental  $\gamma p$  differential cross section up to  $\omega \approx 300 \text{ MeV}$ , thereby extending the domain of applicability of chiral EFT into the Delta region. At the same time we also find reasonable values for the nucleon polarizabilities.

In the next section we introduce the Lagrangian for the Delta and discuss its properties. Section III then describes the  $\delta$ -expansion for Compton scattering on the proton. In particular, we show that for  $\omega \sim m_\pi$  the power counting is very similar to that of HB $\chi$ PT, while for  $\omega \sim \Delta$  the power counting mandates resummation of the  $\Delta$  propagator, thereby

dressing the  $\Delta$  and giving it a finite width. In Section IV we summarize the elements of our calculation, and then in Section V we present and discuss the results of our NLO calculation for the differential cross section, as well as for the spin-independent polarizabilities  $\alpha_p$ ,  $\beta_p$ . We conclude in Section VI.

## II. THE CHIRAL LAGRANGIAN

The pion-nucleon sector of the HB $\chi$ PT Lagrangian is well discussed in the literature, see e.g. [19]. The terms relevant for our purposes are [48] :

$$\begin{aligned} \mathcal{L} = & \frac{1}{2} D_\mu^{ab} \pi_a D^{\mu bc} \pi_c - \frac{1}{2} m_\pi^2 \pi^2 + \bar{N} \left[ i\gamma \cdot D - M_N - \frac{g_A}{2f_\pi} (\gamma \cdot D \pi_a) \tau_a \gamma_5 + \frac{\kappa}{4M_N} \gamma^{\mu\nu} F_{\mu\nu} \right] N \\ & - \frac{e^2}{32\pi^2 f_\pi} F_{\mu\nu} \tilde{F}^{\mu\nu} \pi_3 + \dots, \end{aligned} \quad (8)$$

where  $\pi_a$  represents the isovector pseudoscalar pion field,  $N$  is the isodoublet spinor field of the nucleon,  $\tau_a$  are the isospin Pauli matrices,  $D_\mu = \partial_\mu - ieQA_\mu$ , with  $Q$  representing the electric charge isospin operator ( $Q_\pi = -i\varepsilon^{ab3}$ ,  $Q_N = \frac{1}{2}(1 + \tau_3)$ ),  $A_\mu$  the electromagnetic field,  $F_{\mu\nu} = \partial_\mu A_\nu - \partial_\nu A_\mu$ ,  $\tilde{F}^{\mu\nu} = \frac{1}{2}\varepsilon^{\mu\nu\alpha\beta} F_{\alpha\beta}$ , and  $\kappa$  is the anomalous magnetic moment of the nucleon ( $\kappa_p \simeq 1.79$ ,  $\kappa_n \simeq -1.91$ ).

Next we specify the terms involving the Delta field. Describing the Delta field by an isospin-3/2 spin-3/2 Rarita-Schwinger (RS) vector-spinor  $\Delta_\mu(x)$ , we write the Delta piece of the chiral Lagrangian in the following form:

$$\mathcal{L} = \mathcal{L}_{RS} + \mathcal{L}_{\pi N\Delta} + \mathcal{L}_{\gamma N\Delta} + \dots, \quad (9)$$

$$\mathcal{L}_{RS} = \bar{\Delta}_\mu (i\gamma^{\mu\nu\alpha} \partial_\alpha - M_\Delta \gamma^{\mu\nu}) \Delta_\nu, \quad (10)$$

$$\mathcal{L}_{\pi N\Delta} = \frac{ih_A}{2f_\pi M_\Delta} \bar{N} T_a^\dagger \gamma^{\mu\nu\lambda} (\partial_\mu \Delta_\nu) \partial_\lambda \pi^a + \text{H.c.}, \quad (11)$$

$$\mathcal{L}_{\gamma N\Delta} = \frac{3e}{2M_N(M_N + M_\Delta)} \bar{N} T_3^\dagger (ig_M \tilde{F}^{\mu\nu} - g_E \gamma_5 F^{\mu\nu}) \partial_\mu \Delta_\nu + \text{H.c.} \quad (12)$$

These are the free spin-3/2 Lagrangian, and the  $\pi N\Delta$ ,  $\gamma N\Delta$  couplings respectively. Here  $T_a$  are the isospin 1/2 to 3/2 transition matrices satisfying  $T_a^\dagger T_b = \frac{2}{3}\delta_{ab} - \frac{1}{3}i\varepsilon_{abc}\tau_c$ .

We have kept only the couplings that are linear in the  $\Delta$  field and lowest order in the pion and the photon fields. In principle, there are many other couplings ( $\pi\pi NN$ ,  $\pi\pi N\Delta$ ,  $\gamma\Delta\Delta$ , etc.), represented in Eqs. (8) and (9) by the dots, that are required by the chiral and electromagnetic-gauge symmetries. However, they are not relevant for our calculation at the order we will be considering.

For the purposes of power counting we rearrange the interaction Lagrangian according to the number of small quantities (momentum, pion mass, and factors of  $e$ ) that each term carries:

$$\begin{aligned} \mathcal{L}_I &= \sum_i \mathcal{L}^{(i)}, \\ \mathcal{L}^{(1)} &= -\frac{g_A}{2f_\pi} \bar{N} (\gamma \cdot \partial \pi_a) \tau_a \gamma_5 N + \frac{ieQ_\pi g_A}{2f_\pi} \bar{N} \gamma \cdot A \pi \tau \gamma_5 N + e \bar{N} Q_N \gamma \cdot A N + \mathcal{L}_{\pi N\Delta}, \\ \mathcal{L}^{(2)} &= \frac{\kappa}{4M_N} \bar{N} \gamma^{\mu\nu} N F_{\mu\nu} + \frac{1}{2} (ie Q_\pi \pi A \cdot \partial \pi + \text{H.c.}) + e^2 Q_\pi^2 A^2 \pi \pi + \mathcal{L}_{\gamma N\Delta}^{(gM)}, \end{aligned} \quad (13)$$

$$\begin{aligned}\mathcal{L}^{(3)} &= \mathcal{L}_{\gamma N\Delta}^{(gE)}, \\ \mathcal{L}^{(4)} &= -\frac{e^2}{32\pi^2 f_\pi} F_{\mu\nu} \tilde{F}^{\mu\nu} \pi_3.\end{aligned}$$

### A. Spin-3/2 gauge invariance

It is important to note that our  $N\Delta$  couplings, besides being chiral and gauge invariant, are invariant under the following local (gauge) transformation of the spin-3/2 field:

$$\Delta_\mu(x) \rightarrow \Delta_\mu(x) + \partial_\mu \epsilon(x), \quad (14)$$

where  $\epsilon$  is a spinor. This invariance ensures that the spin-3/2 field has the correct number of spin degrees of freedom (i.e.,  $2s + 1 = 4$ ), cf. [27, 28].

As the result of this additional symmetry, any vertex involving a Delta field,  $\Gamma^\mu(p, \dots)$ , with  $\mu$  being the vector index and  $p$  the 4-momentum of the Delta, will obey the *transversality condition*:

$$p_\mu \Gamma^\mu(p, \dots) = 0. \quad (15)$$

Using the well-known form of the spin-3/2 propagator:

$$S^{\mu\nu}(p) = \frac{1}{\not{p} - M_\Delta} \left[ -g^{\mu\nu} + \frac{1}{3} \gamma^\mu \gamma^\nu + \frac{1}{3M_\Delta} (\gamma^\mu \not{p}^\nu - \gamma^\nu \not{p}^\mu) + \frac{2}{3M_\Delta^2} \not{p}^\mu \not{p}^\nu \right]. \quad (16)$$

it is easy to show that the spin-1/2 sector of the RS propagator decouples [28] and one may equivalently use the following propagator:

$$\tilde{S}_{\mu\nu}(p) = \frac{-1}{\not{p} - M_\Delta} \mathcal{P}_{\mu\nu}^{(3/2)}(p) \quad (17)$$

where  $\mathcal{P}_{\mu\nu}^{(3/2)}(p) = g_{\mu\nu} - \frac{1}{3} \gamma_\mu \gamma_\nu - \frac{1}{3p^2} (\not{p} \gamma_\mu \not{p}_\nu + p_\mu \gamma_\nu \not{p})$  is the spin-3/2 projection operator.

As a matter of fact, it is then also possible to replace the vertices as follows:

$$\tilde{\Gamma}_\mu(p, \dots) = \mathcal{P}_{\mu\nu}^{(3/2)} \Gamma^\nu(p, \dots). \quad (18)$$

In this theory  $\tilde{\Gamma}$  and  $\Gamma$  are completely equivalent. Nevertheless, vertices  $\tilde{\Gamma}$  are sometimes more convenient in actual calculations. For example, the  $\pi N\Delta$  vertex from Eq. (11):

$$\Gamma^\mu(p, k) = (g/M_\Delta) \gamma^{\mu\alpha\beta} p_\alpha k_\beta, \quad (19)$$

where  $g \equiv h_A/2f_\pi$  and  $k$  is the pion 4-momentum, can be replaced by

$$\tilde{\Gamma}_\mu(p, k) = (g/M_\Delta) \not{p} \mathcal{P}_{\mu\nu}^{3/2}(p) k^\nu, \quad (20)$$

where we have used:  $p^\mu \mathcal{P}_{\mu\nu}^{3/2}(p) = 0 = \gamma^\mu \mathcal{P}_{\mu\nu}^{3/2}(p)$ . Furthermore, using  $\mathcal{P}^{3/2} \mathcal{P}^{3/2} = \mathcal{P}^{3/2}$  and  $[\not{p}, \mathcal{P}^{3/2}(p)] = 0$ , Delta-exchange amplitudes are computed effortlessly, e.g.,

$$\Gamma^\mu(p, k') S_{\mu\nu}(p) \Gamma^\nu(p, k) = \tilde{\Gamma}^\mu(p, k') \tilde{S}_{\mu\nu}(p) \tilde{\Gamma}^\nu(p, k) = \frac{-g^2}{\not{p} - M_\Delta} \frac{p^2}{M_\Delta^2} \mathcal{P}_{\mu\nu}^{(3/2)}(p) k'^\mu k^\nu. \quad (21)$$

## B. Relation to conventional $\Delta$ couplings

Our  $N\Delta$  couplings are rather different from the usual ones of, e.g. Refs. [13, 19, 22–24]. As a rule, standard couplings do not have the spin-3/2 gauge symmetry (14). Exceptions are the  $\gamma N\Delta$  coupling of Jones and Scadron [30], which obviously satisfies (15), and the couplings used by Kondratyuk and Scholten [15]. We have adopted the Jones and Scadron convention for the magnetic (M1) coupling,  $g_M$  in Eq. (12).

Other conventional couplings, including the  $G_1, G_2$  representation of the  $\gamma N\Delta$  vertex, do not have the spin-3/2 gauge symmetry. As a result they involve the unphysical lower-spin sectors of the spin-3/2 field, and hence observables become dependent on arbitrary “spin-1/2 backgrounds” associated with “off-shell parameters” of the Delta. Other pathologies (see Ref. [27] and references therein)—all of which can be traced back to the fact that the couplings violate the degrees-of-freedom-counting constraints of the free theory—also occur in these theories.

One can establish a relation between the “inconsistent” and “consistent” couplings using field transformations [31], but this relation holds only in perturbation theory [49] and so is not strictly applicable when resummation of the Delta contributions is necessary, as is the case in the computation of the next section.

## III. COMPTON AMPLITUDE IN THE $\delta$ -EXPANSION

In Compton scattering the momenta of the particles are characterized by the photon energy  $\omega$ . For very low photon energies pions can be “integrated out” of the theory with all non-analytic effects associated with their production being replaced by a power series in  $\omega/m_\pi$  (see, for instance Refs. [32]). Clearly, the condition for this EFT to be effective is  $\omega \ll m_\pi$ . If, instead, we want to develop an EFT for  $\omega \sim m_\pi$  we must treat both  $\omega$  and  $m_\pi$  as low-energy scales, which means that pions must appear in the theory as explicit degrees of freedom.

Similarly for the next relevant scale:  $\Delta \equiv M_\Delta - M_N \approx 293$  MeV. A theory which does not treat it as a low-energy scale is effective only for  $\omega \ll \Delta$ .  $\chi$ PT without explicit Deltas is an example of such an EFT. There only  $m_\pi$  is treated as a small scale, and it is assumed that  $\omega \sim m_\pi \ll \Delta$ . To extend this description to the Delta region,  $\omega \sim \Delta$ , we need to adopt  $\Delta$  as a low-energy scale and include the Delta as an explicit degree of freedom. Thus, we naturally arrive at the scale hierarchy:

$$m_\pi \ll \Delta \ll \Lambda. \quad (22)$$

This hierarchy complies with the assumption of  $\chi$ PT:  $m_\pi \ll \Delta$ , and so  $\chi$ PT still gives the dominant effects in the theory if  $\omega \sim m_\pi$ . At the same time (22) allows us to extend  $\chi$ PT to the Delta region.

In developing our power counting below, we will often keep the dependence of amplitudes on  $m_\pi$  and  $\Delta$  explicit, so that the behavior of the amplitudes in the (independent) chiral ( $m_\pi \rightarrow 0$ ) or the large- $N_c$  ( $\Delta \rightarrow 0$ ) limits is manifest [33]. Nevertheless, for the purposes of assigning an overall size to the amplitude arising from a particular graph or set of graphs we would like to have one expansion parameter:

$$\delta \equiv \frac{\Delta}{\Lambda} \approx \frac{m_\pi}{\Delta}, \quad (23)$$

where we conservatively adopt  $\Lambda \approx 600$  MeV, the scale introduced by the excitation energy of the next baryon resonance. In fact,  $\Lambda$  will represent not only this scale but all of the various high-energy scales, such as  $m_\rho$ ,  $M_N$ ,  $M_\Delta$ , and  $4\pi f_\pi$ . Obviously, in this counting,  $\Delta$  scales as  $\delta$ , while  $m_\pi$  scales as  $\delta^2$ .

While  $\delta$  is of order one half, the expansion in powers of  $\delta$ , is, in principle, no worse than  $\chi$ PT, which is an expansion in  $m_\pi/\Delta$ , or the SSE [24], which is an expansion in powers of  $\Delta/\Lambda$ . Note that, since Eq. (23) is not necessarily true in worlds with other values of  $N_c$ ,  $m_q$ , etc., once that equation is employed, the connection to the limits  $m_q \rightarrow 0$  and  $N_c \rightarrow \infty$  is lost unless the chiral and large- $N_c$  limits are taken simultaneously with  $m_\pi N_c^2$  held fixed.

We assign to each graph an overall  $\delta$ -counting index,  $\alpha$ , which simply tells us that the graph is of size  $e^2 \delta^\alpha / \Lambda$ . Because we deal with two different low-energy scales in our EFT, the index  $\alpha$  has two different expressions, depending on whether the photon energy  $\omega$  is in the vicinity of  $m_\pi$  or  $\Delta$ . For a graph with  $L$  loops,  $N_\pi$  pion propagators,  $N_N$  nucleon propagators,  $N_\Delta$  Delta propagators, and  $V_i$  vertices of dimension  $i$ , the index is

$$\alpha = \begin{cases} 2\alpha_{\chi PT} - N_\Delta, & \omega \sim m_\pi; \\ \alpha_{\chi PT} - N_\Delta, & \omega \sim \Delta, \end{cases} \quad (24)$$

where  $\alpha_{\chi PT} = \sum_i iV_i - 2 + 4L - N_N - 2N_\pi$  is the index of the graph in  $\chi$ PT without explicit Deltas.

In deriving this power-counting we have used the fact that no graphs containing vertices with powers of  $m_\pi^2$  or  $\Delta$  occur up to the order to which we work. Such vertices do arise in higher-order graphs though. In general then, a vertex with  $j$  derivatives,  $k$  insertions of the quark mass, and  $l$  powers of the  $\Delta$ -N mass difference scales as  $\omega^j m_\pi^{2k} \Delta^l$ , and so has overall dimension  $i = j + 2k + l$ . Denoting the number of such vertices by  $V_{jkl}$ , the  $\delta$ -index of an arbitrary graph is:

$$\alpha = \begin{cases} \sum_{jkl} (2j + 4k + l)V_{jkl} + 2(4L - N_N - 2N_\pi - 2) - N_\Delta, & \omega \sim m_\pi; \\ \sum_{jkl} (j + 4k + l)V_{jkl} + 4L - 2 - N_N - 2N_\pi - N_\Delta, & \omega \sim \Delta, \end{cases}$$

which obviously reduces to Eq. (24) if only vertices with  $k = l = 0$  are present.

In the region  $\omega \sim \Delta$ , there is an important exception to this scaling rule: graphs that are one-Delta-reducible (O $\Delta$ R), such as those in Fig. 1, scale not as  $\delta^\alpha$  but as

$$\delta^\alpha \left( \frac{1}{\omega - \Delta} \right)^{N_{O\Delta R}}, \quad (25)$$

where  $N_\Delta$  in the equation for  $\alpha$  now counts only the one-Delta-irreducible propagators, while  $N_{O\Delta R}$  is the number of O $\Delta$ R propagators. In the low-energy region this does not affect the power-counting, however in the region  $\omega \sim \Delta$  these graphs can be dramatically enhanced. This forces us to resum all the O $\Delta$ R contributions, which amounts to dressing the Delta propagator, thus ameliorating the divergence which otherwise occurs at the Delta pole, and producing a width for the Delta of roughly the experimentally-observed size.

Details of the dressing are given below. By definition, once dressing is performed a O $\Delta$ R graph can have only one Delta propagator, and such a graph then scales as:

$$\delta^\alpha \left( \frac{1}{\omega - \Delta - \Sigma} \right), \quad (26)$$

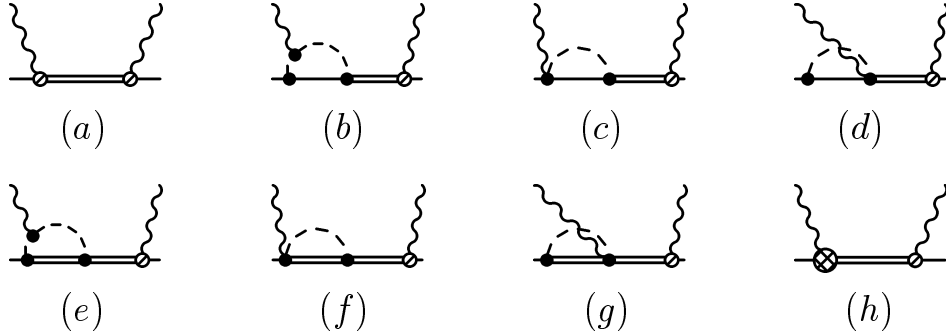


FIG. 1: Eight graphs which are one-Delta-reducible (O $\Delta$ R) and so become enhanced in the region  $\omega \sim \Delta$ . The sliced vertex is the M1  $\gamma N\Delta$  vertex, while the sliced and diced  $\gamma N\Delta$  vertex is the E2 coupling from  $\mathcal{L}^{(3)}$ . Solid dots represent couplings from  $\mathcal{L}^{(1)}$ .

where  $\Sigma$  is the self-energy. The expansion for  $\Sigma$  begins at  $\delta^3$ , and so in the domain  $|\omega - \Delta| \sim \delta^3$  the O $\Delta$ R graphs are enhanced by  $\delta^{-2}$  over the value expected from Eq. (24). Thus, the correct index of a O $\Delta$ R graph in the region  $\omega \sim \Delta$  is

$$\alpha = \alpha_{\chi\text{PT}} - N_{\Delta} - 2. \quad (27)$$

As a result, for instance, the  $s$ -channel-pole Delta graph of Fig. 1(a), which is the simplest O $\Delta$ R graph, is promoted from NNLO in the low-energy region to LO in the Delta region.

The rest of this section is organized as follows: before giving a detailed explanation of Compton counting in the  $\delta$ -expansion we make a few comments on how our scheme compares to standard HB $\chi$ PT and to the SSE of Ref. [23, 24]. We then discuss power counting for the low-energy region  $\omega \sim m_{\pi}$ . In subsection III C we explain the central issue for the higher-energy domain  $\omega \sim \Delta$ : the dressing of the Delta pole. Then in subsection III D we elucidate the impact of this dressing on the counting for Compton scattering graphs.

### A. Comparison with HB $\chi$ PT/SSE

In HB $\chi$ PT the Delta is not included as an explicit “low-energy” degree of freedom in the Lagrangian. Instead it is integrated out of the theory, producing a low-energy theory that, in principle, breaks down for  $\omega \sim \Delta$ . Power counting of graphs is then performed in terms of the index  $q$ , where

$$q \equiv \frac{\omega}{\Lambda} \sim \frac{m_{\pi}}{\Lambda}, \quad (28)$$

where  $\Lambda$  is usually assumed to be of order 1 GeV, although the omission of explicit Deltas suggests instead  $\Lambda \sim \Delta$ .

Hemmert *et al.* [23, 24] introduced the “small-scale expansion” (SSE) (see also the earlier Ref. [29]), where the EFT expansion parameter is:

$$\epsilon \equiv \frac{m_{\pi}}{\Lambda}, \frac{\omega}{\Lambda}, \frac{\Delta}{\Lambda}. \quad (29)$$

The SSE treats  $m_{\pi}$  and  $\Delta$  as the same scale, and hence the Delta must be included explicitly in both energy domains:  $\omega \sim m_{\pi}$  and  $\omega \sim \Delta$ .



This overemphasizes the importance of the Delta somewhat at low energies. In contrast, in the low-energy region, the  $\delta$ -expansion amplitude is akin to that of HB $\chi$ PT. In the region  $\omega \sim \Delta$  the dressing of the Delta implemented here is not performed in either HB $\chi$ PT—naturally, since Deltas are “high-energy” degrees of freedom—or the SSE—as for  $\omega \sim \Delta \sim m_\pi$  all  $\pi N$  loop effects are a small correction to the “bare” Delta propagator.

The table below summarizes the relationship of the  $\delta$ -expansion to HB $\chi$ PT and the SSE.

Expansion	$m_\pi/\Lambda$	$\Delta/\Lambda$
HB $\chi$ PT	$q$	1
SSE	$\epsilon$	$\epsilon$
$\delta$ -expansion	$\delta^2$	$\delta$

TABLE I: The three different expansion discussed in the text. In all three cases the small expansion parameter is of order 1/2, and  $\Lambda$  is the breakdown scale of the theory.

### B. Power counting for $\omega \sim m_\pi$

Here we make the identification  $\omega, m_\pi \sim \delta^2$ . Graphs without Delta propagators then scale exactly as in  $\chi$ PT, but with small momenta  $q \equiv \delta^2$  [50]. The general index of such a graph is then given by Eq. (24). The leading contribution then comes from the sum of the relativistic nucleon Born graph (with  $V_1 = 2$ ,  $N_N = 1$ ,  $L = N_\pi = N_\Delta = 0$ ) depicted in Fig. 2(a) and its crossed partner. Both graphs behave as  $e^2/\omega \sim \delta^{-2}$  as  $\omega \rightarrow 0$ . But the divergent parts cancel in the sum, as the low-energy theorem tells us they must [34]. The dominant term for small  $\omega$  is given by the “Thomson amplitude”:

$$T^{(\text{Th})} = -\frac{(\mathcal{Z}e)^2}{M_N} \varepsilon' \cdot \varepsilon, \quad (30)$$

with  $\varepsilon$  and  $\varepsilon'$  the photon’s initial- and final-state polarization vectors. This, obviously, is  $O(\delta^0)$ .

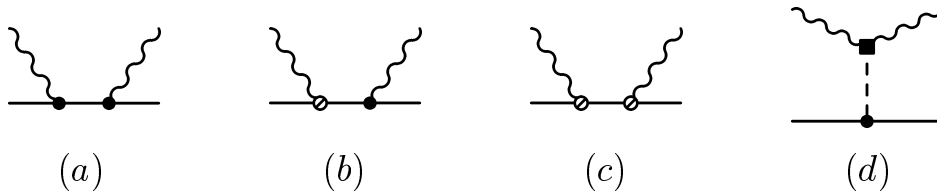


FIG. 2: The four relativistic tree-level graphs without Deltas that are included in our calculation. (We also include graphs generated from these graphs by crossing and/or time reversal.) The dot is the leading-order  $\gamma NN$  coupling, while the sliced vertex is the anomalous-magnetic-moment vertex from  $\mathcal{L}^{(2)}$ . The square indicates the  $\pi^0 \rightarrow \gamma\gamma$  vertex from  $\mathcal{L}^{(4)}$  which generates the chiral anomaly.

When the expansion of the relativistic graphs Fig. 2(a) and 2(b) in powers of  $\omega$  is made there are also pieces  $\sim e^2\omega = O(\delta^2)$ . These form part of the NLO amplitude. The rest of the NLO amplitude is obtained from graphs which have index  $\alpha = 2$ : nucleon tree graphs

with the anomalous magnetic moment coupling (i.e.,  $V_2 = 2$ ,  $N_N = 1$ ,  $L = N_\pi = N_\Delta = 0$ ), see Fig. 2(c), and the  $\pi^0$  exchange graph 2(d), involving the WZW anomaly, which has  $V_1 = V_4 = 1$ ,  $N_\pi = 1$ ,  $L = N_N = N_\Delta = 0$ .

Next we consider  $\pi N$ -loop contributions to  $\gamma N$  scattering. After making a heavy-baryon expansion of our relativistic Lagrangian, in order to avoid difficulties with the appearance of the scale  $M_N$  inside loops [51], we construct the leading loop graphs from vertices in  $\mathcal{L}^{(1)}$ . This yields the graphs of Fig. 3, together with their crossed partners, as reviewed in Ref. [19]. These graphs are specified by  $L = 1$ ,  $N_N = 1$ ,  $N_\Delta = 0$  and either  $V_1 = V_2 = 2$ ,  $N_\pi = 3$  or  $V_1 = 2$ ,  $N_\pi = 1$  or  $V_1 = 2$ ,  $V_2 = 1$ ,  $N_\pi = 2$ , and hence all have  $\alpha = 2$ . They are the only loop graphs with this counting index if we adopt Coulomb gauge and employ the heavy-baryon expansion. Explicit computation [17, 19] reveals that the sum of these graphs indeed produces a Compton amplitude that behaves as:

$$T^{(\pi N \text{ loop})} = \frac{e^2}{(4\pi f_\pi)^2} \frac{\omega^2}{m_\pi} F^{(1)}\left(\frac{\omega}{m_\pi}\right), \quad (31)$$

where  $F^{(1)}$  is a non-analytic function whose form is given in detail for the various possible spin and polarization structures in Refs. [17, 19] and in Appendix A.  $F^{(1)}$  has the property that  $F^{(1)} \sim 1$  for  $\omega \lesssim m_\pi$ . A crucial feature of Eq. (31) is the fact that the sum of these leading loop graphs is proportional to  $\omega^2$ . This is also a consequence of the low-energy theorem [34].

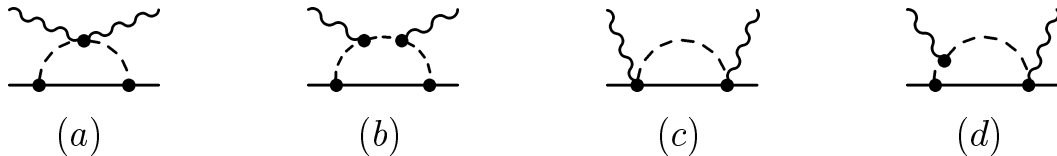


FIG. 3: The dominant  $\pi N$ -loop contributions to  $\gamma N$  scattering (crossed and time-reversed partners are not shown, but are included).

The counting formula (24) indicates that loop graphs with insertions from the second-order  $\chi$ PT Lagrangian  $\mathcal{L}^{(2)}$  are down by two further powers of  $\delta$ , being of  $O(\delta^4)$ . Relativistic corrections to Eq. (31) are suppressed by  $\omega/M$ , and so are also  $O(\delta^4)$ . Some loop graphs at  $O(\delta^4)$  require renormalization, and the corresponding counterterms must be included. Meanwhile, graphs with two  $\pi N$  loops are  $O(\delta^6)$  in this counting. Thus—at least in this energy domain—it is not until  $O(\delta^6)$  that two-pion intermediate states contribute to the  $\gamma N$  amplitude. And graphs involving additional  $\pi N$  rescatterings are similarly suppressed. Considering more loops and/or insertions with more derivatives only serves to further increase the  $\delta$ -index of graphs. Thus unitarity (in both the  $\pi N$  and  $\pi\pi N$  channels) is violated in our calculation, but the violation is always an effect of an order beyond that at which we work.

Graphs containing the Delta begin to contribute at  $O(\delta^3)$ . The tree graph with two M1  $\gamma N \Delta$  vertices—see Fig. 1(a)—has  $\alpha = 3$  ( $V_2 = 2$ ,  $N_\Delta = 1$ ,  $L = N_N = N_\pi$ ). Meanwhile, the counting of the one- $\pi\Delta$ -loop graphs, Fig. 4, is analogous to that for the  $\pi N$  loops, the only difference being that now  $N_N = 0$ ,  $N_\Delta = 1$  instead of  $N_N = 1$ ,  $N_\Delta = 0$ . This results in the sum of the graphs in Fig. 4 being  $O(\delta^3)$ , i.e. scaling as:

$$T^{(\Delta\pi \text{ loop})} = \frac{e^2}{(4\pi f_\pi)^2} \frac{\omega^2}{\Delta} H^{(1)}\left(\frac{\omega}{\Delta}, \frac{m_\pi}{\Delta}\right), \quad (32)$$

where  $H^{(1)}$  is a non-analytic function which is of order 1 for  $m_\pi/\Delta \sim \delta$ , and  $\omega/\Delta \lesssim 1$ . Equation (32) is consistent with the low-energy theorem, and agrees with the explicit computation performed for these loops in Ref. [24].

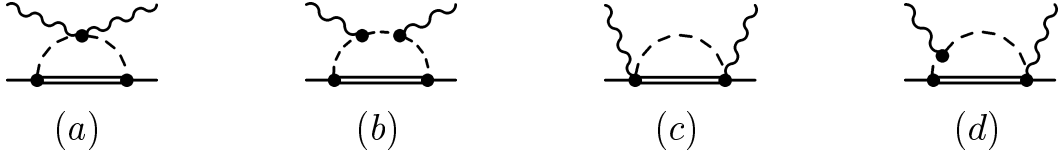


FIG. 4: The dominant  $\pi\Delta$ -loop contributions to  $\gamma N$  scattering. Again, graphs generated from these by crossing and/or time-reversal are not shown.

In summary: in the  $\delta$ -expansion the Thomson term is the leading mechanism for Compton scattering on the nucleon at low energies,  $\omega \sim m_\pi$ . In this region pion loops are suppressed by one power of  $\omega \sim m_\pi \sim \delta^2$ , exactly as in HB $\chi$ PT. If explicit Deltas are included in the theory the leading Delta-pole and  $\Delta\pi$ -loop graphs are suppressed by  $\delta^3$  relative to leading. They thus occur one order higher in the  $\delta$ -expansion than the  $N\pi$  loop graphs of Fig. 3. They are, however, still one power of  $\delta^{-1}$  larger than graphs arising from  $\mathcal{L}^{(2)}$  insertions in  $\pi N$  loop graphs.

### C. Dressing the Delta

The key issue for the theory in the region  $\omega \sim \Delta$  is the treatment of the Delta pole. One- $\Delta$ -reducible (O $\Delta$ R) graphs must be resummed in order to remove the divergence which otherwise occurs when  $\not{p} = M_\Delta$ .

Formally, all O $\Delta$ R graphs can be summed via the series:

$$S_{\mu\nu}(p) = S_{\mu\nu}^{(0)}(p) + S_{\mu\mu'}^{(0)}(p) \Sigma^{\mu'\nu'}(p) S_{\nu'\nu}^{(0)}(p) + \dots, \quad (33)$$

where  $\Sigma^{\mu\nu}(p)$  is the full one-Delta-irreducible (O $\Delta$ I) Delta self-energy, and  $S_{\mu\nu}(p)$  ( $S_{\mu\nu}^{(0)}(p)$ ) is the dressed (bare) Delta propagator.

The function  $\Sigma_{\mu\nu}$  has a  $\delta$ -expansion of its own:

$$\Sigma_{\mu\nu} = \Sigma_{\mu\nu}^{(3)} + \Sigma_{\mu\nu}^{(4)} + \dots \quad (34)$$

This expansion begins at  $O(\delta^3)$ , with the graphs depicted in Fig. 5, together with the counterterms necessary for their renormalization. Insertions from  $\mathcal{L}_{\pi N}^{(2)}$  generate effects in  $\Sigma^{(4)}$ . These effects include relativistic corrections to the leading heavy-baryon result  $\Sigma^{(3)}$ . Two-loop contributions to the self-energy—including the leading effect of the  $N\pi\pi$  channel—first occur in  $\Sigma^{(5)}$ , and are thus smaller by  $\delta^2$  than the dominant piece of  $\Sigma$ .

If:

$$|\omega - \Delta| \sim \delta^3 \quad (35)$$

and we keep only the third-order piece of the self-energy then all terms on the right-hand side of Eq. (33) are the same order. A perturbative expansion of the right-hand side—which

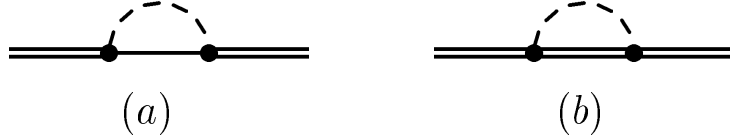


FIG. 5:  $\pi N$  and  $\pi\Delta$  contributions to the  $\Delta$  self-energy  $\Sigma$ . The vertices are from  $\mathcal{L}^{(1)}$  and so both graphs are  $O(\delta^3)$ .

is certainly valid for  $|\omega - \Delta| \sim \delta^2$  or larger—is no longer appropriate. Instead, if (35) holds, the whole series must be resummed, giving:

$$S_{\mu\nu}(p) = \frac{-1}{\not{p} - M_\Delta - \bar{\Sigma}^{(3)}(p)} \mathcal{P}_{\mu\nu}^{(3/2)}(p). \quad (36)$$

Eq. (35) then defines precisely what we mean by  $\omega \sim \Delta$ .

In fact the most general Lorentz-covariant form of  $\Sigma^{\mu\nu}(p)$  is rather complicated: it contains up to 10 independent scalar functions. As a result the dressed propagator does not generally have the form (36). This is a consequence of using “inconsistent” spin-3/2 couplings—ones that *do not* obey the symmetry under (14). If, however, couplings which are consistent in that sense are used then the Delta self-energy can be written as:

$$\Sigma^{\mu\nu}(p) = \Sigma(p) \mathcal{P}^{(3/2)\mu\nu}(p), \quad (37)$$

with  $\Sigma(p)$  akin to the usual fermion self-energy:  $\Sigma(p) = A(p^2) \not{p} + B(p^2)$ , where  $A$  and  $B$  are scalar functions. Dressing then affects only the spin-3/2 piece of the propagator and the form (36) results. The divergence at  $\not{p} = M_\Delta$  is ameliorated, and no further resummation is necessary.  $\delta$ -counting indicates that the effects of  $\Sigma^{(n)}$  for  $n \geq 4$  can be included by perturbing around the propagator (36).

Delta propagators of this form have been used in other authors’ extensions of chiral perturbation theory to the resonance region [36–38], although in these works it is not clear why only the spin-3/2 sector is dressed. Note that in contrast to the work of, for instance, Ref. [37], we do not dress the nucleon pole by  $\pi N$  loops. Arguments analogous to those of this subsection suggest that nucleon dressing is only necessary from a power-counting point of view for  $\omega \sim 0$ , and there  $\Sigma(p)$  is purely real. As we shall now see, after renormalization the real part of  $\Sigma^{(3)}$  plays a negligible role in the propagator (36).

In Eq. (36) the quantity  $\bar{\Sigma}^{(3)}$  indicates that we are resumming the renormalized third-order Delta self-energy. The explicit renormalization of this quantity will be performed elsewhere. Here we make a more general argument which constrains the form and importance of any renormalized self-energy appearing in Eq. (36).

First, observe that the general Lorentz structure of the self-energy  $\Sigma$  results in:

$$S_{\mu\nu}(p) = -\frac{Z(p^2)}{\not{p} - M(p^2)} \mathcal{P}_{\mu\nu}^{(3/2)}(p), \quad (38)$$

with  $Z$  and  $M$  scalar functions of  $p^2$ . After mass, wave function, and coupling constant renormalization these can be written as:

$$Z(p^2) = 1 + (p^2 - M_\Delta^2) f_Z(p^2) + i \text{Im } Z(p^2); \quad (39)$$

$$M(p^2) = M_\Delta + (p^2 - M_\Delta^2)^2 f_M(p^2) + i \text{Im } M(p^2), \quad (40)$$

with  $f_Z$  and  $f_M$  real functions of  $p^2$ .

Substituting these forms into Eq. (38) we find that:

$$S_{\mu\nu}(p) = -\frac{1 + i \operatorname{Im} Z(p^2)}{\not{p} - M_\Delta - i \operatorname{Im} M(p^2)} \mathcal{P}_{\mu\nu}^{(3/2)}(p) + O\left(\frac{1}{\Lambda}\right). \quad (41)$$

In the region (35) the pole piece is  $O(\delta^{-3})$ , while the remaining ‘‘background’’ terms are  $O(\delta^0)$ . Thus any corrections to  $S_{\mu\nu}(p^2)$  from  $\operatorname{Re} Z(p^2)$  or  $\operatorname{Re} M(p^2)$  are three powers of  $\delta$  beyond leading. Corrections from  $\operatorname{Im} Z(p^2)$  are equally suppressed, since it too is  $O(\delta^3)$ .

Thus, up to corrections which are N<sup>3</sup>LO, it is sufficient to compute only  $\operatorname{Im} M(p^2)$ . Provided that  $\omega \leq \Delta + m_\pi$  this comes exclusively from Fig. 5(a). A straightforward calculation gives:

$$\operatorname{Im} M(s) \equiv -\frac{\Gamma(s)}{2} = -\left(\frac{h_A}{2f_\pi}\right)^2 \frac{s + M_N^2 - m_\pi^2}{24\pi M_\Delta^2} k^3 \theta(k), \quad (42)$$

where  $k$  is the on-shell value of the pion three-momentum:

$$k = \{[s - (M_N + m_\pi)^2][s - (M_N - m_\pi)^2]/(4s)\}^{1/2} \sim \delta. \quad (43)$$

Thus, the width is  $O(\delta^3)$ , as promised.

The final form of the resummed  $\Delta$  propagator is then:

$$S_{\mu\nu}(p) = -\frac{1}{\not{p} - M_\Delta + \frac{i}{2}\Gamma(p^2)} \mathcal{P}_{\mu\nu}^{(3/2)}(p), \quad (44)$$

If this propagator appears in a O $\Delta$ R  $\gamma$ N graph and (35) is satisfied then it scales as  $\delta^{-3}$ .

#### D. Power counting for $\omega \sim \Delta$

The effect of this modified scaling for the Delta propagator is that (dressed) O $\Delta$ R graphs become the dominant effects for  $\omega \sim \Delta$ . Their  $\delta$ -index is given by Eq. (27). The Delta-pole graph Fig. 1(a), with M1  $\gamma N\Delta$  vertices (i.e.,  $V_2 = 2$ ,  $N_\Delta = 1$ ), has  $\alpha = -1$  in the region (35) and gives the leading contribution there. The graph of Fig. 1(h) with one E2-coupling (i.e.,  $V_2 = 1$ ,  $V_3 = 1$ ) has  $\alpha = 0$ , and hence is of next-to-leading order (NLO) if  $\omega \sim \Delta$ .

Meanwhile the O $\Delta$ R graphs of Fig. 1(b)–(g) (and their time-reversed partners) are characterized by  $L = N_N = N_\Delta = 1$  and either  $V_1 = V_2 = N_\pi = 2$  or  $V_2 = N_\pi = 1$ ,  $V_1 = 2$ . They too have  $\alpha = 0$  and contribute at NLO. These loop graphs are divergent and must be renormalized. This is achieved via graph 1(h). The loop effects may then be included in the calculation by the use of an energy-dependent E2-coupling:  $g_E \rightarrow g_E(s)$ . The leading effect here again arises from the imaginary part of the loops, hence:

$$g_E(s) = g_E + i \left(\frac{g_A h_A}{4f_\pi^2}\right) \frac{s + M_N^2 - m_\pi^2}{24\pi s} \frac{M_N k^2}{\omega_\gamma} \frac{2M_N(M_N + M_\Delta)}{3M_\Delta \omega_\gamma} [Q_0(\omega_k/k) - Q_2(\omega_k/k)] \theta(k), \quad (45)$$

where  $\omega_\gamma = (s - M_N^2)/2\sqrt{s}$ ,  $\omega_k = \sqrt{m_\pi^2 + k^2}$ , while  $k$  is given by Eq. (43), and  $Q_l$  is the  $l$ th Legendre function of the second kind.

NLO effects can also be obtained by considering corrections from  $\Sigma^{(4)}$  to the leading Delta self-energy  $\Sigma^{(3)}$ . More complicated electromagnetic couplings and higher-order terms in  $\Sigma$  lead to effects of NNLO in the  $\delta$ -expansion of O $\Delta$ R graphs.

What is the  $\delta$ -index of graphs without a Delta pole? O $\Delta$ I graphs such as  $\Delta\pi$  and  $N\pi$  loops obey Eq. (24)—they are not enhanced. They retain a positive  $\delta$  index, and so are at least NNLO in this counting.

One might wonder how to reconcile this with Eq. (31) which seems to suggest that the  $\delta$ -scaling of the dominant  $\pi N$  loops will be, for  $\omega \sim \Delta$ :

$$e^2 \frac{\omega^2}{m_\pi} = e^2 \frac{\Delta^2}{\Delta^2} = e^2 \delta^0. \quad (46)$$

This conclusion is erroneous because  $F^{(1)}$  is not  $O(1)$  if  $\omega/m_\pi$  is large. If  $\omega/m_\pi \gg 1$  the loop functions should be expanded about the large- $\omega$  limit, not the small  $\omega$  one, and doing so results in:

$$T^{(\pi N \text{ loop})} = \frac{e^2}{(4\pi^2 f_\pi)^2} \left[ c_1 \omega + d_1 m_\pi + c_3 \frac{m_\pi^2}{\omega} + c_5 \frac{m_\pi^4}{\omega^3} + \dots \right]. \quad (47)$$

Assigning  $\omega \sim \Delta$ ,  $m_\pi \sim \Delta^2$  we see that this series, rather than one in increasing powers of  $\omega$  is the correct one for the “medium-energy” regime  $\omega \sim \Delta \gg m_\pi$ . This is completely opposite to a polarizability expansion in increasing powers of  $\omega$ . In our approach  $\omega \sim \Delta$  is sufficiently far from threshold that a power-series expansion around  $\omega = 0$  of Delta contributions is not very enlightening.

## IV. IN PRACTICE

### A. Defining the NLO calculation

To perform a complete NLO calculation in the whole energy region,  $0 < \omega \lesssim \Delta$ , we include all of the nucleon pole and  $\pi N$  loop graphs of Figs. 2 and 3, together with their crossed partners. To these we add the O $\Delta$ R graphs of Fig. 1, which in the low-energy region contribute at NNLO and above, but for  $|\omega - \Delta| \sim \delta^3$  give effects of leading and next-to-leading order. We also include the O $\Delta$ R graph with two  $g_E \gamma N \Delta$  couplings, even though it is formally NNLO.

We keep all of these effects in both kinematic regions. Note that this means we are always keeping contributions that are, strictly speaking, beyond the order to which we work. This is done in order to provide a smooth transition between the two different photon energy domains. For the same reason, in both regions we always use the resummed Delta propagator (44).

The power counting of Sec. III C indicates that at NLO we must include effects due to the  $O(\delta^4)$  piece of  $\Sigma$ ,  $\Sigma^{(4)}$ . The heavy-baryon graphs which contribute to the  $O(\epsilon^4)$  self-energy in a heavy-baryon calculation with explicit Deltas [40] are shown in Fig. 6. The relativistic calculation of the Delta width that led to Eq. (42) already includes the effects of the graphs (a) and (b). As for graph (c), this graph gives a contribution to  $\Sigma$  which behaves as [40]:

$$\Sigma^{6(c)}(p) \sim \frac{(b_3 + b_8)h_A}{f_\pi^2} \int \frac{d^4 k}{(2\pi)^4} \frac{k^2}{k^2 - m_\pi^2} \frac{v \cdot k}{v \cdot (p - k)}. \quad (48)$$

The imaginary part of this graph is proportional to  $\omega k m_\pi^2$  (with  $k$  given by Eq. (43)), so while it is  $O(\epsilon^4)$  in the SSE, in our counting it is  $O(\delta^6)$ , and so well beyond the order to

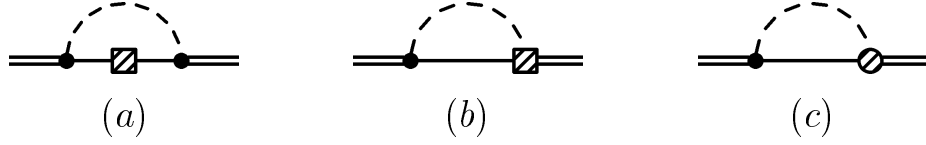


FIG. 6: Heavy-baryon expansion graphs that represent  $O(\epsilon^4)$   $\pi$ N-loop contributions to the  $\Delta$  self-energy  $\Sigma$ . The sliced squares are vertices from the second-order  $\pi N\Delta$  HB Lagrangian whose coefficient is fixed by Lorentz invariance. The sliced circle represents a vertex from  $\mathcal{L}_{\pi N\Delta}$  with a coefficient which is *a priori* undetermined (see Ref. [40]).

which we work. Thus the result (42) is already accurate up to corrections of relative order  $\delta^2$ .

The  $u$ -channel Delta-pole graph is NNLO throughout this entire energy region and is *not* included in our Compton amplitude. Therefore, by looking at its effect on cross sections we can estimate the importance of NNLO contributions.

## B. Covariant decomposition of the Compton amplitude

To compute the amplitude of Compton-scattering on a spin-1/2 target in a manifestly Lorentz and gauge invariant form, we specify it in terms of eight scalar amplitudes  $A_1 \dots A_8$  (instead of the usual six):

$$M_{fi} = e^2 \bar{u}(p') \sum_{i=1}^8 A_i(s, t) O_i^{\mu\nu} \mathcal{E}'_{\mu}(q') \mathcal{E}_{\nu}(q) u(p) \quad (49)$$

where  $p'$ ,  $p$  (and  $q'$ ,  $q$ ) are the final and initial 4-momenta of the nucleon (and photon), respectively;  $u$  is the free nucleon spinor,  $\mathcal{E}_{\mu}$  is a modified photon polarization vector:

$$\mathcal{E}_{\mu}(q) = \varepsilon_{\mu} - \frac{P \cdot \varepsilon}{P \cdot q} q_{\mu}, \quad (50)$$

with  $P = p + p'$ . Tensors  $O_i$  are given by:

$$\begin{aligned} O_1^{\mu\nu} &= -g^{\mu\nu} \\ O_2^{\mu\nu} &= q^{\mu} q'^{\nu} \\ O_3^{\mu\nu} &= -\gamma^{\mu\nu} \\ O_4^{\mu\nu} &= g^{\mu\nu} (q' \cdot \gamma \cdot q) \\ O_5^{\mu\nu} &= q^{\mu} q'_{\alpha} \gamma^{\alpha\nu} - \gamma^{\mu\alpha} q_{\alpha} q'^{\nu} \\ O_6^{\mu\nu} &= q^{\mu} q'_{\alpha} \gamma^{\alpha\nu} - \gamma^{\mu\alpha} q_{\alpha} q'^{\nu} \\ O_7^{\mu\nu} &= q^{\mu} q'^{\nu} (q' \cdot \gamma \cdot q) \\ O_8^{\mu\nu} &= i\gamma_5 \epsilon^{\mu\nu\alpha\beta} q'_{\alpha} q_{\beta}. \end{aligned} \quad (51)$$

Mandelstam variables  $s$ ,  $t$ ,  $u$  are defined as usual:

$$\begin{aligned} s &= (p + q)^2 = M_N^2 + 2p \cdot q \\ t &= (q' - q)^2 = -2q \cdot q' \\ u &= (p - q')^2 = M_N^2 - 2p \cdot q' \end{aligned} \quad (52)$$

where we have used the onshell conditions:  $q^2 = q'^2 = 0$ ,  $p^2 = p'^2 = M_N^2$ . Note that  $P \cdot q = \frac{1}{2}(s - u) = P \cdot q'$ .

The representation (49) is obtained by writing down the most general covariant structure (for the onshell situation) and imposing the electromagnetic current-conservation condition. Thus this representation incorporates both covariance and gauge-invariance in a manifest way.

The amplitudes  $A_i$  are most easily computed in the following Lorenz-invariant gauge:

$$P \cdot \varepsilon = 0 = P \cdot \varepsilon'. \quad (53)$$

This condition can also be achieved in the Coloumb gauge ( $\varepsilon_0 = 0 = \varepsilon'_0$ ) by going to the Breit frame:  $\vec{P} = 0$ .

In the Coloumb gauge, the structures  $O_1$ – $O_6$  exactly match the ones in the standard decomposition (e.g. [19, 34]), while  $O_7$  and  $O_8$  can be reduced to linear combinations of  $O_3$ ,  $O_5$  and  $O_6$ :

$$O_7 = (\omega^2 + \frac{1}{2}t)[-tO_3 + O_5] - \omega^2O_6, \quad (54)$$

$$O_8 = \frac{1}{2}\omega(-tO_3 + O_5 - O_6). \quad (55)$$

In particular, the results for the nucleon-exchange (Born) graphs, the anomaly graph, and the Delta exchange graphs are specified in terms of the amplitudes  $A_1, \dots, A_8$  in Appendix A. As our calculation of these graphs is fully relativistic, it differs from that of HB $\chi$ PT in Refs. [19, 23] by terms of  $O(\delta)$ .

Meanwhile, for the  $\pi N$  loop graphs depicted in Fig. 3, we have used the  $O(q^3)$  HB $\chi$ PT result of Refs. [17, 19]. This is done in order to avoid difficulties with the treatment of the nucleon-mass-scale  $M_N$  inside the loops. The amplitude obtained in a fully-relativistic calculation of these loops would differ from the result used here by terms of  $O(\omega/M)$  and  $O(m_\pi/M)$ , i.e. terms down by  $\delta^2$ . The loop contributions are given in Appendix A.

We do include one particular relativistic effect because we write the photon energy  $\omega$  that appears in the loop functions as  $\omega = \sqrt{s} - M_N$ . The standard choices for  $\omega$ —c.m. photon energy [19], Breit-frame photon energy [17]—differ from this by terms which are of N<sup>3</sup>LO in our counting. We adopt this prescription in order to ensure that the Compton amplitude's  $\pi N$  cut occurs at the correct value of  $s$ .

## V. RESULTS AND DISCUSSION

### A. Differential cross sections for $\gamma p$ scattering

There are no  $\gamma N$  contact terms at NLO in the  $\delta$ -expansion. This leaves us with three EFT parameters which must be fixed using the data:  $g_E$ ,  $g_M$ , and  $h_A$ . For  $h_A$  we adopt the phenomenological value  $h_A = 2.81$  ( $f_{\pi N \Delta}^2/4\pi \simeq 0.35$ ), which corresponds to a Delta width  $\Gamma(M_\Delta^2) \simeq 111$  MeV—consistent with the range given by the Particle Data Group [39]. This value of  $h_A$  is roughly 5% larger than that obtained from the large- $N_c$  relation  $h_A = \frac{3}{\sqrt{2}}g_A$ .

This leaves us with two free parameters:  $g_M$  and  $g_E$  of the  $\gamma N \Delta$  coupling (12). They represent the strength of, respectively, the M1 and E2  $\gamma N \rightarrow \Delta$  transitions.



In principle these are relatively well known from pion photoproduction. In particular, their ratio is related to the  $R_{EM} = E2/M1$  ratio:

$$R_{EM} = \frac{g_E \Delta}{2g_M(M_N + M_\Delta) - g_E \Delta} \times 100\%. \quad (56)$$

The determination of this ratio has recently been the subject of experimental programs at JLab and MAMI. The present PDG value is  $R_{EM} = (-2.5 \pm 1.0)\%$  [39]. However, this number is measured only indirectly through the extraction of the ratio of the pion-photoproduction multipoles at the Delta-resonance position. These multipoles are affected by a number of background processes and the relationship (56) is only strictly true at leading order in the  $\delta$ -expansion for the  $\gamma p \rightarrow \pi p$  amplitude. To fully understand the constraint that pion photoproduction places on  $g_E/g_M$  in this EFT a higher-order calculation of  $\gamma p \rightarrow \pi p$  using the  $\delta$ -expansion is necessary. (For an attempt to compute this process in the SSE see Ref. [41].) Absent such a calculation, here we regard  $g_M$  and  $g_E$  as free parameters and fit them to get the best agreement with  $\gamma p$  cross-section data. An important future test of the usefulness of the  $\delta$ -expansion will be whether the resultant value for  $g_E/g_M$  is ultimately consistent with that found from pion photoproduction data using the same framework.

The results for the differential cross section at several different energies are presented in Figs. 7 and 8. The long-dashed orange curve represents a calculation which includes only the Born graphs of Fig. 2. The dashed blue curve is the result when the  $\pi N$  loops of Fig. 3 are added, and so gives the  $O(q^3)$  prediction of HB $\chi$ PT. Finally, the complete NLO calculation in the  $\delta$ -expansion is represented by the solid red curve. The sharp rise at backward angles as  $\omega$  increases past the pion-production threshold is now reproduced in the theory. This sharp rise is very difficult to obtain in  $\chi$ PT without explicit Deltas.

In Figs. 7 and 8 we also show a theoretical error band, demarcated by the red dots. This is obtained by estimating the size of the NNLO contribution in the following way:

$$T(\text{theor. err.}) = -\frac{e^2}{M_N} \varepsilon' \cdot \varepsilon \times \begin{cases} \omega^2/\Delta, & \omega \sim m_\pi \\ \omega, & \omega \sim \Delta. \end{cases} \quad (57)$$

The error band in Figs. 7 and 8 is plotted with the border between the two kinematic domains at  $\omega = 200$  MeV. The band is an estimate of how far we expect the NNLO corrections to change the results. It may overestimate the theoretical error since our calculation already includes a number of NNLO contributions: relativistic effects coming from tree graphs, Delta-exchange—which is NNLO for  $\omega \sim m_\pi$ —and  $\pi N$  loops—which are NNLO for  $\omega \sim \Delta$ .

The fit of the cross section favors the following values for the  $\gamma N \rightarrow \Delta$  parameters:

$$g_M = 2.6 \pm 0.2, \quad g_E = -6.0 \pm 0.9, \quad (58)$$

The solid line in Figs. 7 and 8 gives the result for the central values of  $g_M$  and  $g_E$ . The uncertainty in Eq. (58) is found by varying these couplings until the experimental cross section in the Delta region is no longer within the theoretical error band.

The resulting value of  $g_M$  is consistent with the large  $N_c$  value:  $g_M = \frac{2\sqrt{2}}{3}(1 + \kappa_p) \simeq 2.63$ , while the value of  $g_E$  is considerably different from phenomenological expectations. For instance, from  $R_{EM} = -2.5\%$  and Eq. (56) one would expect  $g_E = -1$ . This problem dramatizes the importance of performing an analogous calculation of pion photoproduction to check the consistency of the  $\delta$ -expansion.

Next we would like to note that, although formally the imaginary and real parts of  $g_E(s)$  of Eq. (45) are the same order, numerically the imaginary part is smaller by at least a factor of six.  $\text{Im } g_E(s)$  has a negligible impact on the angular distributions shown in Figs. 7 and 8.

The NLO prediction for the differential cross section's energy-dependence is shown in Fig. 9 for a scattering angle of  $90^\circ$ . The solid purple line is the result when only  $\Delta$ -pole mechanisms are included and  $g_M$  and  $g_E$  are chosen according to (58). The solid red line gives the result of our NLO calculation. Individual contributions from Born graphs and  $\pi N$  loops are given by the orange dashed and green short-dashed lines respectively. The  $O(q^3)$  prediction of HB $\chi$ PT is represented by the blue dashed line. This figure shows our NLO calculation of the Delta width is in good agreement with the data. This lends support to our adoption of the value  $h_A = 2.81$ . However, it must be pointed out that since our EFT was only designed for  $0 \leq \omega \lesssim \Delta$  the agreement at the higher energies which is seen in Fig. 9 is probably somewhat fortuitous.

## B. Polarizabilities

The results for the nucleon polarizabilities are worked out in Appendix B. The leading contribution to polarizabilities is from  $\pi N$  loops and hence is exactly the same as in HB $\chi$ PT, see Eq. (1). On the other hand, our results for the Delta contributions differ from earlier ones in several ways:

1. First of all, in contrast to the results of Refs. [13, 22], they are independent of “off-shell parameters”.
2. The leading SSE result of Ref. [23] for the magnetic polarizability is also free of off-shell parameters (in the SSE they enter at NLO). Formally, the result of Appendix B agrees with that found in Ref. [23]—apart from a higher-order relativistic effect which is numerically only of order 10%:

$$\beta_N^{(\Delta) \text{ this work}} = \frac{2}{2 + \Delta} \beta_N^{(\Delta) \text{ SSE}}.$$

However, our fit to the cross section prefers a significantly smaller value of the  $\gamma N \Delta$  coupling than was used in Ref. [23] and this leads to a markedly smaller numerical result for  $\beta_p^{(\Delta)}$ .

3. Perhaps most importantly, our NLO calculation includes neither  $u$ -channel Delta-exchange nor  $\pi \Delta$  loops, since both are NNLO in the  $\delta$ -expansion. In fact, the Delta contributions quoted in Appendix B stem from both the  $s$ - and  $u$ -channel Delta exchange graphs. However, the NLO calculation presented above has no  $u$ -channel graph. Thus to find the polarizabilities that correspond to the cross-section calculation of the previous subsection one must halve the Delta pieces of polarizabilities given in Appendix B.

All of these effects produce a Delta-contribution to the magnetic polarizability that is significantly smaller than that found in previous EFT calculations with explicit Deltas [21–23, 25]:

$$\beta_p^{(\Delta)} = \frac{\alpha g_M^2}{(M_N + M_\Delta)^2 \Delta} = (2.7 \pm 0.4) \times 10^{-4} \text{ fm}^3. \quad (59)$$

The Delta contribution to the electric polarizability comes solely from the  $s$ -channel Delta-pole with two  $g_E$  couplings:

$$\alpha_p^{(\Delta)} = -\frac{\alpha g_E^2}{(M_N + M_\Delta)^3} = (-2.0 \pm 0.7) \times 10^{-4} \text{ fm}^3. \quad (60)$$

The observant reader will have noticed that the inclusion of  $\Delta$  contributions in the polarizabilities is not, strictly speaking, consistent at NLO in our power counting. The  $s$ -channel Delta pole is, like its  $u$ -channel counterpart, NNLO for  $\omega \sim 0$ . In spite of this we have included the Delta contributions in the results shown in Table II. The numbers there represent the polarizabilities corresponding to the cross-section calculation already presented.

We expect that in an NNLO  $\delta$ -expansion calculation the Delta's effect on  $\beta_p$  will roughly double.  $\alpha_p$  will also be modified, thanks to the graphs in Fig. 4 and the  $u$ -channel Delta-pole graph with two  $g_E$  couplings. Estimating these effects gives the theory error bars which appear in the second line of the table. We note that, even though NNLO effects make a significant difference in the values for  $\alpha_p$  and  $\beta_p$ , their impact on the low-energy differential cross section is not large, being represented by the theoretical error band in Fig. 7. This suggests that the extraction of polarizabilities from Compton data is a delicate process.

Reference	$\alpha_p$	$\beta_p$
NLO HB $\chi$ PT [19]	12.2	1.2
NLO $\delta$ [this work]	$10.2^{+4.2}_{-2.0}$	$3.9^{+2.7}_{-0.4}$
NLO SSE [25]([23])	16.4 (20.8)	9.1 (14.7)
PDG average [39]	$12.0 \pm 0.7$	$1.6 \pm 0.6$
LEGS [4]	$11.8 \pm 2.0$	$1.4 \pm 1.5$
MAMI [5]	$11.9 \pm 2.1$	$1.2 \pm 1.4$
Beane <i>et al.</i> [20]	$12.1 \pm 1.6$	$3.2 \pm 1.2$

TABLE II: Proton polarizabilities in  $\chi$ PT, the  $\delta$ -expansion, and the SSE, compared to values extracted from experiment. Results are in units of  $10^{-4} \text{ fm}^3$ .

## VI. CONCLUDING REMARKS

The expansion developed in this paper for the  $\gamma$ N amplitude is based on the scale hierarchy  $m_\pi \ll \Delta \ll \Lambda$ . The EFT expansion parameter employed here is  $\delta$ , which represents both the ratio of  $m_\pi$  to  $\Delta$  and the ratio of  $\Delta$  to  $\Lambda$ . The success of the resulting “ $\delta$ -expansion” is to be judged by its efficacy as an EFT of Compton scattering.

The existence of two different low-energy scales in the theory forces us to develop independent power countings for the two different photon-energy regimes. For  $\omega \sim m_\pi$  the Compton amplitude obtained is exactly that of  $\chi$ PT up to effects from the Delta which are down by  $\delta^3$  relative to leading. On the other hand, if  $\omega \sim \Delta$ ,  $O\Delta R$  graphs dominate the Compton amplitude. Resummation of the Delta self-energy is necessary in these graphs. The Delta propagator appearing in them acquires a finite, energy-dependent, width. Up to effects suppressed by  $\delta^3$  this is the only correction to the Delta propagator that is necessary. Vertex corrections also appear at NLO in this region.

We performed a calculation of the  $\gamma N$  amplitude which includes all effects that are of leading or next-to-leading order in the region  $\omega \sim m_\pi$ , as well as all effects that are of leading or next-to-leading order in the region  $\omega \sim \Delta$ . The sum of all of these pieces of the amplitude defines our NLO calculation. Thus, in each of the two regions considered, mechanisms of NNLO in that particular region are included in the calculation. Nevertheless, effects of relative order  $\delta^3$  (e.g.  $\Delta\pi$  loops) are omitted in the low-energy region, while effects of relative order  $\delta^2$  (e.g. two-loop dressing of the Delta) are omitted in the higher-energy domain. These neglected effects define the theoretical error bar of our calculation.

Note that in this calculation tree-level graphs are computed relativistically, while for loop graphs we use the HB $\chi$ PT result. While this gives the correct  $\gamma N$  amplitude up to the order to which we work, a fully-relativistic treatment of  $\pi N$  loops would be more aesthetically pleasing.

After fitting the only two free parameters in our theory, the E2 and M1  $\gamma N \Delta$  couplings, good agreement with the low-energy  $\gamma p$  data is found. The spin-independent polarizabilities  $\alpha$  and  $\beta$  that result from our NLO calculation are in reasonable agreement with contemporary extractions from data [5, 20].

The development of the  $\delta$ -expansion opens up a number of avenues for further study. Higher-order calculations of Compton scattering on the nucleon will be necessary to see if the good agreement found at NLO persists, and if the expansion in powers of  $\delta$  is well-behaved or not. Also, the use of the  $\delta$ -expansion in other processes, e.g. pion photoproduction, is an important potential future application. Indeed, the EFT presented here should ultimately be judged by its success in simultaneously describing data on nucleon Compton scattering, pion photoproduction, and  $\pi N$  scattering. Only then can the reliability of the EFT, and hence of our extraction of  $g_E$  and  $g_M$  from  $\gamma N$  data to NLO in the  $\delta$ -expansion, really be judged.

The use of the  $\delta$ -expansion in two-nucleon systems might also reap significant rewards. We plan to use the amplitude developed here, together with consistent two-body currents, in a calculation of  $\gamma D$  scattering [42]. It is also possible that the  $\delta$  expansion could be profitably employed to organize the Delta contributions to the chiral nucleon-nucleon potential developed in Refs. [43–45].

## Acknowledgments

We thank Sergey Kondratyuk and Olaf Scholten for comments on the manuscript. D. R. P. thanks Harald Griebhammer and Thomas Hemmert for useful discussions and the Benasque Centre for Science for its hospitality during part of this work. This research was supported by the U. S. Department of Energy under grants DE-FG02-93ER40756, DE-FG02-02ER41218, and by the National Science Foundation under grant NSF-SGER-0094668.

## APPENDIX A: RESULTS FOR COMPTON INVARIANT AMPLITUDES

We define the photon energy as:  $\omega = (p \cdot q)/M_N = (s - M_N^2)/2M_N$ . The results for the invariant amplitudes are presented in the nucleon mass units ( $M_N = 1$ ). Below  $\mathcal{Z} = 1$  for the proton,  $\mathcal{Z} = 0$  for the neutron. Expressions for the Delta-exchange are obtained using the algebraic manipulation program Form [46].

**1. Nucleon  $s$ -channel:**

$$\begin{aligned}
A_1(\omega, t) &= -\frac{1}{2} \left[ \mathcal{Z}^2 + \frac{1}{4} (\mathcal{Z} + \kappa)^2 t + \frac{1}{2} \kappa^2 (\omega + \frac{1}{4} t) \right] \\
A_2(\omega, t) &= -\frac{\kappa}{2\omega} \left[ \mathcal{Z} + \frac{1}{2} \kappa (1 + \frac{1}{4} \omega + \frac{1}{8} t) \right] \\
A_3(\omega, t) &= A_1(\omega, t) \\
A_4(\omega, t) &= -\frac{1}{4\omega} \left[ (\mathcal{Z} + \kappa)^2 + \frac{1}{2} \kappa^2 \omega \right] \\
A_5(\omega, t) &= \frac{(\mathcal{Z} + \kappa)^2}{4\omega} \\
A_6(\omega, t) &= -\frac{\mathcal{Z}(\mathcal{Z} + \kappa)}{4\omega} \\
A_7(\omega, t) &= \frac{\kappa^2}{16\omega} \\
A_8(\omega, t) &= -A_4(\omega, t)
\end{aligned} \tag{A1}$$

**2.  $\pi^0 \rightarrow \gamma\gamma$  anomaly graph:**

$$A_8(\omega, t) = \frac{g_A}{(2\pi f_\pi)^2} \frac{2\mathcal{Z} - 1}{t - m_{\pi^0}^2}, \quad A_1, \dots, A_7 = 0. \tag{A2}$$

**3. Delta  $s$ -channel:**

$$\begin{aligned}
A_1(\omega, t) &= F(\omega, \Delta) \left\{ \frac{2}{3} (\omega^2 + \frac{1}{2} t) (2 + \Delta) G_M^2 - \frac{2}{3} \omega^2 \Delta G_E^2 \right. \\
&\quad + \frac{2}{3} \omega^3 (G_M^2 + G_E^2 - G_M G_E) + \frac{1}{8} t^2 G_M^2 \\
&\quad \left. + \omega t \left[ (2 + \frac{5}{6} \Delta + \frac{7}{6} \omega + \frac{1}{4} t) G_M^2 - \frac{1}{6} (2 + \Delta + \omega) G_M G_E + \frac{1}{6} \omega G_E^2 \right] \right\} \\
A_2(\omega, t) &= F(\omega, \Delta) \left\{ -\frac{2}{3} (2 + \Delta) G_M^2 - \frac{1}{3} \omega \left[ (8 + 3\Delta) G_M^2 + 2\Delta G_E^2 - (2 + \Delta) G_M G_E \right] \right. \\
&\quad + \omega^2 \left( -\frac{7}{6} G_M^2 + \frac{5}{6} G_E^2 - \frac{2}{3} G_M G_E \right) \\
&\quad \left. + t \left[ -\frac{1}{12} (1 - \Delta) G_M^2 - \frac{1}{12} G_E^2 + \frac{1}{3} \omega \left( -\frac{1}{2} G_M^2 + G_E^2 + \frac{5}{4} G_M G_E \right) + \frac{1}{32} t (G_M + G_E)^2 \right] \right\} \\
A_3(\omega, t) &= F(\omega, \Delta) \left\{ -\frac{1}{3} \omega^2 [2G_M^2 + \Delta (G_M^2 - G_E^2)] - \frac{1}{3} \omega^3 (G_M^2 + G_E^2 - 4G_M G_E) \right. \\
&\quad + t \left[ -\frac{1}{6} (2 + \Delta) G_M^2 + \frac{1}{3} \omega G_M \left( G_M \left( \frac{3}{2} + \Delta \right) + G_E (2 + \Delta) \right) \right. \\
&\quad \left. \left. + \omega^2 \left( \frac{11}{12} G_M^2 - \frac{1}{12} G_E^2 + \frac{1}{3} G_M G_E \right) + \frac{1}{4} t G_M^2 \left( \frac{1}{2} + \omega \right) \right] \right\} \\
A_4(\omega, t) &= F(\omega, \Delta) \left\{ -\frac{1}{3} (2 + \Delta) G_M (G_M + \omega G_E) - \omega \left( 1 + \frac{1}{3} \Delta \right) G_M^2 \right. \\
&\quad \left. + \frac{1}{3} \omega^2 (G_M^2 + G_E^2 - G_M G_E) + \frac{1}{2} t G_M^2 \left( \frac{1}{2} + \omega \right) \right\} \\
A_5(\omega, t) &= F(\omega, \Delta) \left\{ \frac{1}{3} (2 + \Delta) G_M^2 - \frac{1}{6} \omega \left[ 2(1 + \Delta) G_M^2 + \Delta G_E^2 + (2 + \Delta) G_M G_E \right] \right\}
\end{aligned} \tag{A3}$$

$$\begin{aligned}
& - \omega^2 G_M (G_M - G_E) + \frac{1}{4} t \left[ G_M G_E + \frac{1}{2} \Delta G_M (G_M + G_E) - \omega G_M (G_M - G_E) \right] \Big\} \\
A_6(\omega, t) &= F(\omega, \Delta) \left\{ \omega G_M [G_M + \frac{1}{2} \Delta (G_M + G_E)] + \omega^2 G_M (G_M - G_E) \right. \\
& \quad \left. + \frac{1}{4} t \left[ G_M^2 + \frac{1}{2} \Delta G_M (G_M + G_E) + \omega G_M (G_M - G_E) \right] \right\} \\
A_7(\omega, t) &= F(\omega, \Delta) \left\{ (2 + \Delta) \left( \frac{7}{12} G_M^2 + \frac{1}{2} G_M G_E \right) - \frac{1}{12} \Delta G_E^2 \right. \\
& \quad \left. + \omega \left( \frac{7}{12} G_M^2 - \frac{5}{12} G_E^2 - \frac{1}{3} G_M G_E \right) + \frac{1}{16} t (G_M + G_E)^2 \right\} \\
A_8(\omega, t) &= F(\omega, \Delta) \left\{ \frac{4}{3} (2 + \Delta) G_M^2 + \omega \left[ 4 \left( 1 + \frac{1}{3} \Delta \right) G_M^2 - \frac{2}{3} (2 + \Delta) G_M G_E \right] \right. \\
& \quad \left. + \frac{1}{6} \omega^2 (G_M^2 + G_E^2 - 4 G_M G_E) - \frac{1}{2} t G_M^2 \left( \frac{1}{2} + \omega \right) \right\}
\end{aligned}$$

with  $G_{M,E} = \frac{3}{2(2+\Delta)} g_{M,E}$  and

$$F(\omega, \Delta) = -\frac{2}{3} \frac{1}{s - M_\Delta^2 + i M_\Delta \Gamma(s)} = -\frac{2}{3} \frac{1}{2\omega - \Delta(2 + \Delta) + i M_\Delta \Gamma(\omega)}, \quad (\text{A4})$$

where  $\frac{2}{3} = T_3^\dagger T_3$  is the isospin factor, and the width  $\Gamma$  is given by Eq. (42).

The corresponding  $u$ -channel graphs are obtained by crossing so that the crossing-symmetric amplitude is given by

$$\begin{aligned}
& A_i(\omega, t) + A_i(-\omega', t), \quad \text{for } i = 1, 2, 8 \\
& A_i(\omega, t) - A_i(-\omega', t), \quad \text{for } i = 3, \dots, 7
\end{aligned}$$

with  $\omega' = p \cdot q' = (1 - u)/2$ .

#### 4. HB $\chi$ PT $\pi N$ loops

Defining  $\zeta = (\sqrt{s} - M_N)/m_\pi$  and  $\tau = -2\zeta^2(1 - \cos \theta)$ , where  $\theta$  is the center-of-mass angle between the incoming and outgoing photon momenta, one finds [19]:

$$\begin{aligned}
A_1(s, t) &= -\frac{g_A^2 m_\pi}{8\pi f_\pi^2} \left\{ 1 - \sqrt{1 - \zeta^2} + \frac{2 - \tau}{\sqrt{-\tau}} \left[ \frac{1}{2} \arctan \frac{\sqrt{-\tau}}{2} - I_1(\zeta, \tau) \right] \right\}, \\
A_2(s, t) &= -\frac{g_A^2}{8\pi f_\pi^2 m_\pi} \frac{2 - \tau}{(-\tau)^{3/2}} [I_1(\zeta, \tau) - I_2(\zeta, \tau)], \\
A_3(s, t) &= \frac{g_A^2 m_\pi}{8\pi^2 f_\pi^2} \left[ \frac{1}{\zeta} \arcsin^2 \zeta - \zeta + 2\zeta^4 \sin^2 \theta I_3(\zeta, \tau) \right], \\
A_4(s, t) &= \frac{g_A^2}{4\pi^2 f_\pi^2 m_\pi} I_4(\zeta, \tau), \\
A_5(s, t) &= -\frac{g_A^2}{8\pi^2 f_\pi^2 m_\pi} [I_5(\zeta, \tau) - 2\zeta^2 \cos \theta I_3(\zeta, \tau)], \\
A_6(s, t) &= \frac{g_A^2}{8\pi^2 f_\pi^2 m_\pi} [I_5(\zeta, \tau) - 2\zeta^2 I_3(\zeta, \tau)], \tag{A5}
\end{aligned}$$

where

$$\begin{aligned}
I_1(\zeta, \tau) &= \int_0^1 dz \arctan \frac{(1-z)\sqrt{-\tau}}{2\sqrt{1-\zeta^2 z^2}}, \\
I_2(\zeta, \tau) &= \int_0^1 dz \frac{2(1-z)\sqrt{-\tau(1-\zeta^2 z^2)}}{4(1-\zeta^2 z^2) - \tau(1-z)^2}, \\
I_3(\zeta, \tau) &= \int_0^1 dx \int_0^1 dz \frac{x(1-x)z(1-z)^3}{S^3} \left[ \arcsin \frac{\zeta z}{R} + \frac{\zeta z S}{R^2} \right], \\
I_4(\zeta, t) &= \int_0^1 dx \int_0^1 dz \frac{z(1-z)}{S} \arcsin \frac{\zeta z}{R}, \\
I_5(\zeta, t) &= \int_0^1 dx \int_0^1 dz \frac{(1-z)^2}{S} \arcsin \frac{\zeta z}{R}, \tag{A6}
\end{aligned}$$

with

$$S = \sqrt{1 - \zeta^2 z^2 - \tau(1-z)^2 x(1-x)}, \quad R = \sqrt{1 - \tau(1-z)^2 x(1-x)}. \tag{A7}$$

## APPENDIX B: RESULTS FOR POLARIZABILITIES

The nucleon electric ( $\alpha_N$ ) and magnetic ( $\beta_N$ ) polarizabilities:

$$\begin{aligned}
\alpha_N &= \frac{\alpha}{2} \frac{\partial^2}{\partial \omega^2} A_1^{(NB)}(0,0) + \alpha A_2^{(NB)}(0,0) = \frac{5\pi\alpha}{6m_\pi} \left( \frac{g_A}{4\pi f_\pi} \right)^2 - \frac{2\alpha g_E^2}{(M_N + M_\Delta)^3}, \\
\beta_N &= -\alpha A_2^{(NB)}(0,0) = 2\alpha \frac{\partial}{\partial t} A_1^{(NB)}(0,0) = \frac{\pi\alpha}{12m_\pi} \left( \frac{g_A}{4\pi f_\pi} \right)^2 + \frac{2\alpha g_M^2}{(M_N + M_\Delta)^2 \Delta}, \tag{B1}
\end{aligned}$$

where  $A_i^{(NB)}$  are the amplitudes with the Born graphs subtracted.

- 
- [1] E. L. Hallin *et al.*, ‘‘Compton scattering from the proton,’’ *Phys. Rev. C* **48**, 1497 (1993).
  - [2] B. E. MacGibbon, G. Garino, M. A. Lucas, A. M. Nathan, G. Feldman and B. Dolbilkin, ‘‘Measurement of the electric and magnetic polarizabilities of the proton,’’ *Phys. Rev. C* **52**, 2097 (1995) [arXiv:nucl-ex/9507001].
  - [3] G. Blanpied *et al.* [LEGS Collaboration], ‘‘Polarized Compton Scattering From The Proton,’’ *Phys. Rev. Lett.* **76**, 1023 (1996); *ibid.* **79**, 4337 (1997).
  - [4] G. Blanpied *et al.*, ‘‘N  $\rightarrow$  Delta transition and proton polarizabilities from measurements of  $p(\vec{\gamma}, \gamma)$ ,  $p(\vec{\gamma}, \pi^0)$ , and  $p(\vec{\gamma}, \pi^+)$ ,’’ *Phys. Rev. C* **64**, 025203 (2001).
  - [5] V. Olmos de Leon *et al.*, ‘‘Low-Energy Compton Scattering And The Polarizabilities Of The Proton,’’ *Eur. Phys. J. A* **10**, 207 (2001).
  - [6] M. Lucas, Ph. D. Thesis, University of Illinois, unpublished (1994).
  - [7] D. L. Hornidge *et al.*, ‘‘Elastic Compton scattering from the deuteron and nucleon polarizabilities,’’ *Phys. Rev. Lett.* **84**, 2334 (2000) [arXiv:nucl-ex/9909015].
  - [8] M. Lundin *et al.*, ‘‘Compton scattering from the deuteron and neutron polarizabilities,’’ arXiv:nucl-ex/0204014.

- [9] N. R. Kolb *et al.*, “Quasi-free Compton Scattering from the Deuteron and Nucleon Polarizabilities,” *Phys. Rev. Lett.* **85**, 1388 (2000) [arXiv:nucl-ex/0003002].
- [10] K. Kossert *et al.*, “Neutron polarizabilities investigated by quasi-free Compton scattering from the deuteron,” *Phys. Rev. Lett.* **88**, 162301 (2002) [arXiv:nucl-ex/0201015]; “Quasi-free Compton scattering and the polarizabilities of the neutron,” arXiv:nucl-ex/0210020.
- [11] A. I. L’vov, V. A. Petrun’kin and M. Schumacher, “Dispersion theory of proton Compton scattering in the first and second resonance regions,” *Phys. Rev. C* **55**, 359 (1997).
- [12] D. Drechsel, M. Gorchtein, B. Pasquini and M. Vanderhaeghen, “Fixed-t subtracted dispersion relations for Compton scattering off the nucleon,” *Phys. Rev. C* **61**, 015204 (2000).
- [13] V. Pascalutsa and O. Scholten, “On the structure of the  $\gamma N\Delta$  vertex: Compton scattering in the  $\Delta(1232)$  region and below,” *Nucl. Phys. A* **591**, 658 (1995);  
O. Scholten, A. Y. Korchin, V. Pascalutsa and D. Van Neck, “Pion and photon induced reactions on the nucleon in a unitary model,” *Phys. Lett. B* **384**, 13 (1996).
- [14] T. Feuster and U. Mosel, “Photon and meson induced reactions on the nucleon,” *Phys. Rev. C* **59**, 460 (1999) [arXiv:nucl-th/9803057];  
G. Penner and U. Mosel, “Vector meson production and nucleon resonance analysis in a coupled channel approach for energies  $m(N) < \sqrt{s} < 2$  GeV. II: Photon induced results,” arXiv:nucl-th/0207069.
- [15] S. Kondratyuk and O. Scholten, “Compton scattering on the nucleon at intermediate energies and polarizabilities in a microscopic model,” *Phys. Rev. C* **64**, 024005 (2001);  
“Low-energy Compton scattering on the nucleon and sum rules,” *ibid.* **65**, 038201 (2002).
- [16] D. Babusci, G. Giordano and G. Matone, “Chiral perturbation theory and nucleon polarizabilities,” *Phys. Rev. C* **55**, 1645 (1997).
- [17] J.A. McGovern, *Phys. Rev. C* **63**, 064608 (2001).
- [18] V. Bernard, N. Kaiser, and U.-G. Meißner, *Nucl. Phys.* **B383**, 442 (1992); V. Bernard, N. Kaiser, J. Kambor, and U.-G. Meißner, *Nucl. Phys.* **B388**, 315 (1992).
- [19] V. Bernard, N. Kaiser, and U. G. Meißner, “Chiral dynamics in nucleons and nuclei,” *Int. J. Mod. Phys. E* **4**, 193 (1995) [arXiv:hep-ph/9501384].
- [20] S. R. Beane, M. Malheiro, J. A. McGovern, D. R. Phillips, and U. van Kolck, “Nucleon polarizabilities from low-energy Compton scattering”, arXiv:nucl-th/0209002.
- [21] M. N. Butler and M. J. Savage, “Electromagnetic polarizability of the nucleon in chiral perturbation theory,” *Phys. Lett. B* **294**, 369 (1992) [arXiv:hep-ph/9209204];  
M. N. Butler, M. J. Savage and R. P. Springer, “Strong and electromagnetic decays of the baryon decuplet,” *Nucl. Phys. B* **399**, 69 (1993) [arXiv:hep-ph/9211247].
- [22] V. Bernard, N. Kaiser, U. G. Meißner, and A. Schmidt, “Aspects of nucleon Compton scattering,” *Z. Phys. A* **348**, 317 (1994) [arXiv:hep-ph/9311354].
- [23] T. R. Hemmert, B. R. Holstein, J. Kambor, “ $\Delta(1232)$  and the polarizabilities of the nucleon,” *Phys. Rev. D* **55**, 5598 (1997).
- [24] T. R. Hemmert, B. R. Holstein and J. Kambor, “Systematic  $1/M$  expansion for spin  $3/2$  particles in baryon chiral perturbation theory,” *Phys. Lett. B* **395**, 89 (1997); *J. Phys. G* **24**, 1831 (1998).
- [25] T. R. Hemmert, B. R. Holstein, J. Kambor and G. Knochlein, “Compton scattering and the spin structure of the nucleon at low energies,” *Phys. Rev. D* **57**, 5746 (1998) [arXiv:nucl-th/9709063].
- [26] H. W. Grißhammer, T. R. Hemmert, R. Hildebrandt, and B. Pasquini, in preparation.
- [27] V. Pascalutsa, “Quantization of an interacting spin- $3/2$  field and the Delta isobar,” *Phys.*



- Rev. D **58**, 096002 (1998) [arXiv:hep-ph/9802288].
- [28] V. Pascalutsa and R. Timmermans, “Field theory of nucleon to higher-spin baryon transitions,” Phys. Rev. C **60**, 042201 (1999) [arXiv:nucl-th/9905065].
- [29] E. Jenkins and A. V. Manohar, “Baryon Chiral Perturbation Theory Using A Heavy Fermion Lagrangian,” Phys. Lett. B **255**, 558 (1991).
- [30] H. F. Jones and M. D. Scadron, Ann. Phys. **81**, 1 (1973).
- [31] V. Pascalutsa, “Correspondence of consistent and inconsistent spin-3/2 couplings via the equivalence theorem,” Phys. Lett. B **503**, 85 (2001) [arXiv:hep-ph/0008026].
- [32] J. W. Chen, H. W. Griesshammer, M. J. Savage and R. P. Springer, “Gamma deuteron Compton scattering in effective field theory,” Nucl. Phys. A **644**, 245 (1998);  
H. W. Griesshammer and G. Rupak, “Nucleon Polarisabilities from Compton Scattering on the Deuteron,” Phys. Lett. B **529**, 57 (2002).
- [33] R. Flores-Mendieta, C. P. Hofmann, E. Jenkins and A. V. Manohar, “On the structure of large  $N(c)$  cancellations in baryon chiral perturbation theory,” Phys. Rev. D **62**, 034001 (2000);  
T. D. Cohen, “Chiral and large- $N_c$  limits of quantum chromodynamics and models of the baryon,” Rev. Mod. Phys. **68**, 599 (1996) [arXiv:hep-ph/9512275];  
T. D. Cohen and W. Broniowski, “The Role of the delta isobar in chiral perturbation theory and hedgehog soliton models,” Phys. Lett. B **292**, 5 (1992);  
W. Broniowski and T. D. Cohen, “Response of nucleons to external probes in hedgehog models. 1. Electromagnetic polarizabilities,” Phys. Rev. D **47**, 299 (1993);  
T. D. Cohen, “Electromagnetic properties of the Delta in the large  $N(c)$  and chiral limits,” arXiv:hep-ph/0210278.
- [34] F. E. Low, Phys. Rev. **96**, 1428 (1954); M. Gell-Mann and M. L. Goldberger, *ibid.* 1433 (1954).
- [35] T. Becher and H. Leutwyler, “Baryon chiral perturbation theory in manifestly Lorentz invariant form,” Eur. Phys. J. C **9**, 643 (1999) [arXiv:hep-ph/9901384].
- [36] E. Oset, E. Marco, J. C. Nacher, J. A. Oller, J. R. Pelaez, A. Ramos and H. Toki, “Photoproduction of meson and baryon resonances in a chiral unitary approach,” Prog. Part. Nucl. Phys. **44**, 213 (2000);  
U. G. Meissner and J. A. Oller, “Chiral unitary meson baryon dynamics in the presence of resonances: Elastic pion nucleon scattering,” Nucl. Phys. A **673**, 311 (2000);  
A. Gomez Nicola, J. Nieves, J. R. Pelaez and E. Ruiz Arriola, “Improved unitarized heavy baryon chiral perturbation theory for  $\pi N$  scattering,” Phys. Lett. B **486**, 77 (2000).
- [37] M. F. Lutz and E. E. Kolomeitsev, “Relativistic chiral SU(3) symmetry, large  $N(c)$  sum rules and meson baryon scattering,” Nucl. Phys. A **700**, 193 (2002) [arXiv:nucl-th/0105042].
- [38] K. Torikoshi and P. J. Ellis, “Low energy pion nucleon scattering in the heavy baryon and infrared schemes,” arXiv:nucl-th/0208049.
- [39] Particle Data Group, “Review of Particle Physics,” Phys. Rev. D **66**, 010001 (2002).
- [40] N. Fettes and U. G. Meissner, “Pion nucleon scattering in an effective chiral field theory with explicit spin-3/2 fields,” Nucl. Phys. A **679**, 629 (2001) [arXiv:hep-ph/0006299].
- [41] C. W. Kao and T. D. Cohen, “The pion photoproduction in the Delta(1232) region,” Phys. Rev. C **60**, 064619 (1999) [arXiv:nucl-th/9811062].
- [42] H. W. Griesshammer, T. Hemmert, V. Pascalutsa and D. R. Phillips, in progress.
- [43] C. Ordonez, L. Ray and U. van Kolck, “The Two-Nucleon Potential from Chiral Lagrangians,” Phys. Rev. C **53**, 2086 (1996) [arXiv:hep-ph/9511380].
- [44] E. Epelbaum, W. Glockle and U. G. Meissner, “Nuclear forces from chiral Lagrangians using the method of unitary transformation. II: The two-nucleon system,” Nucl. Phys. A **671**, 295

- (2000) [arXiv:nucl-th/9910064].
- [45] D. R. Entem and R. Machleidt, “Accurate nucleon nucleon potential based upon chiral perturbation theory,” *Phys. Lett. B* **524**, 93 (2002) [arXiv:nucl-th/0108057].
- [46] J. A. M. Vermaseren, “Symbolic Manipulation with FORM, version 2,” Computer Algebra Nederland, Amsterdam, 1991.
- [47] Throughout this paper the designations LO, NLO, etc. refer to the order in the  $\gamma N$  amplitude. These one-loop results are, strictly speaking, *leading*-order predictions for  $\alpha_p$  and  $\beta_p$ , but we refer to them as next-to-leading order (NLO) since Eq. (1) is derived by considering the NLO result for the nucleon Compton amplitude.
- [48] Our conventions: metric tensor  $g^{\mu\nu} = \text{diag}(1, -1, -1, -1)$ ;  $\gamma$ -matrices  $\gamma^\mu$ ,  $\gamma^5 = i\gamma^0\gamma^1\gamma^2\gamma^3$ ,  $\{\gamma^\mu, \gamma^\nu\} = 2g^{\mu\nu}$ ; fully antisymmetrized products of  $\gamma$ -matrices  $\gamma^{\mu\nu} = \frac{1}{2}[\gamma^\mu, \gamma^\nu] = \gamma^\mu\gamma^\nu - g^{\mu\nu}$ ,  $\gamma^{\mu\nu\alpha} = \frac{1}{2}\{\gamma^{\mu\nu}, \gamma^\alpha\} = i\varepsilon^{\mu\nu\alpha\beta}\gamma_\beta\gamma_5$ ,  $\gamma^{\mu\nu\alpha\beta} = \frac{1}{2}[\gamma^{\mu\nu\alpha}, \gamma^\beta] = i\varepsilon^{\mu\nu\alpha\beta}\gamma_5$ ; spinor indices are omitted.
- [49] Even then, it holds only if the “naive” Feynman rules apply in the inconsistent theory, which, strictly speaking, is not true [27].
- [50] The electron charge is usually counted as one power of  $q$  in  $\chi$ PT, and thus  $O(q^3) = O(e^2q)$  for Compton scattering. Here we do not count the factor of  $e^2$  that is present in all Compton graphs when assessing the  $\delta$ -index of a graph.
- [51] The ideal solution to this difficulty would be to use infrared regularization [35] to compute the  $\pi N$  loops. But the result of such a computation should only differ from the HB $\chi$ PT one by terms suppressed by  $\delta$ . Such terms are higher order than we are considering here.

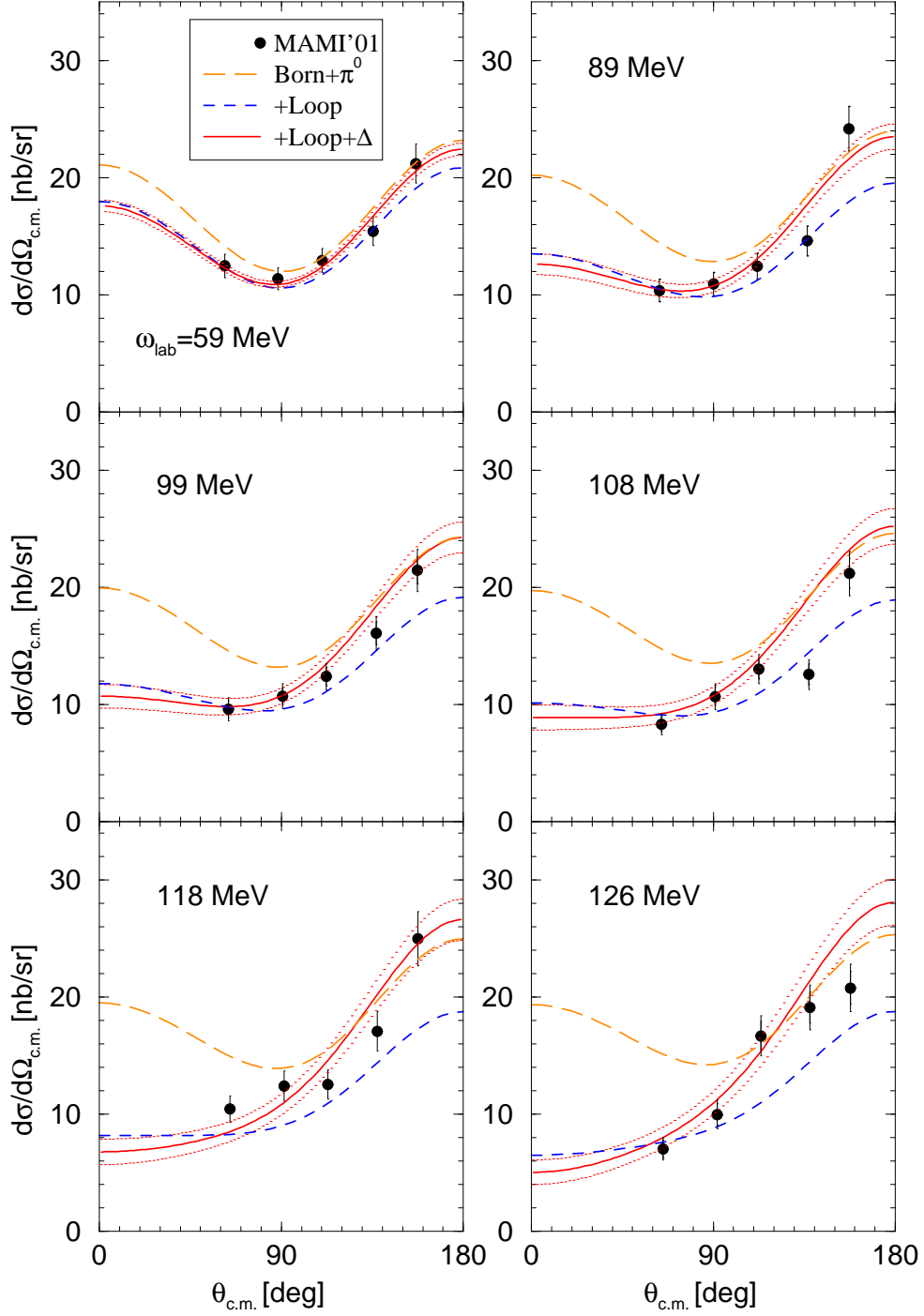


FIG. 7: Angular distribution of the  $\gamma p$  differential cross section at low energies. Data points are from Ref. [5]. The long-dashed orange line represents the sum of nucleon and pion Born graphs, the blue dashed line gives the NLO  $\chi$ PT prediction, and the red solid line is the full result at NLO in the  $\delta$ -expansion. The dots give an estimate of the theoretical error.

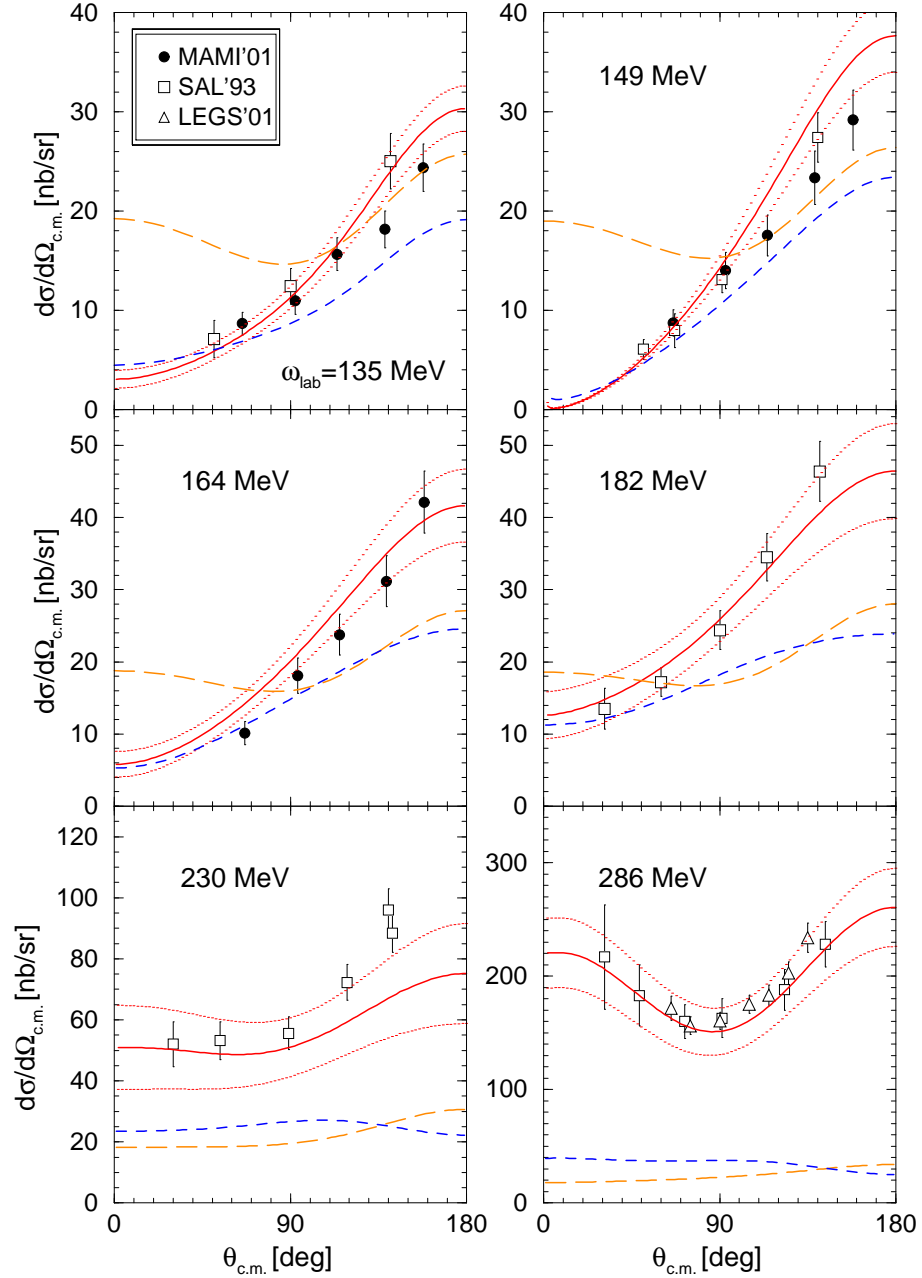


FIG. 8: Angular distribution of the  $\gamma p$  differential cross section. Legend for the curves is the same as in Fig. 7. Data points are from Refs. [5] – MAMI'01, [1] – SAL'93, [4] – LEGS'01.

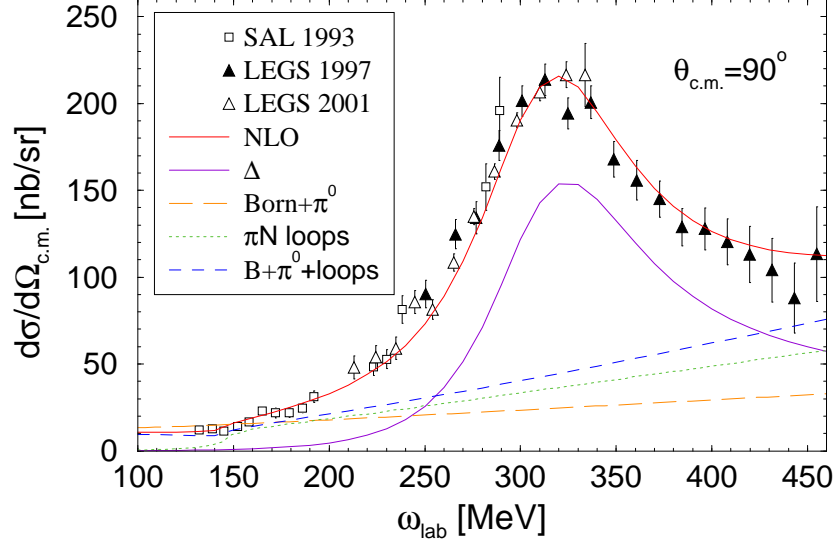


FIG. 9: Energy dependence of the  $\gamma p$  differential cross section at  $90^\circ$ . Data points are from Refs. [1] – SAL’93, [3] – LEGS’97, and [4] – LEGS’01. The red solid, orange long-dashed, and blue dashed lines are as above, while the purple curve now gives the contribution arising solely from the Delta, and the green short-dashed curve is the effect of  $\pi N$  loops alone.